**CERIUM OXIDE THIN FILM GROWTH USING
PULSED ELECTRON DEPOSITION METHOD**

Thekra Abdelqader Radwan Alqutamy
Master's thesis
Graduate School of Natural and Applied Sciences
Department of Nanoscience and Nanoengineering
Supervisor: Assoc. Prof. Dr. Mustafa Tolga YURTCAN
2024

CERIUM OXIDE THIN FILM GROWTH USING PULSED ELECTRON DEPOSITION METHOD

(Darbeli Elektron Biriktirme Yöntemiyle Seryum Oksit İnce Film Büyütülmesi)

MASTER'S THESIS

Thekra Abdelqader Radwan Alqutamy

Supervisor: Assoc. Prof. Dr. Mustafa Tolga YURTCAN

Erzurum

August, 2024

RECORD OF ACCEPTANCE AND APPROVAL

The thesis titled "Cerium Oxide Thin Film Growth Using Pulsed Electron Deposition Method" prepared by Thekra Alqutamy has been found successful and accepted as a master's thesis in the Department of Nanoscience and Nanotechnology by our committee on the date of the thesis defense examination, 29/08/2024.

Chair: Prof. Dr. Özlem BARIŞ   Aslı ıslak imzalıdır
Atatürk University

Supervisor: Assoc. Prof. Dr. M. Tolga YURTCAN   Aslı ıslak imzalıdır
Atatürk University

Jury Member: Asst. Prof. Dr. Erdal İĞMAN   Aslı ıslak imzalıdır
Bayburt University

The decision of the Institute Board of Directors dated .. / .. / …. and numbered ……………..

I certify that this thesis fulfills the requirements specified in the relevant articles of the Atatürk University Graduate Education and Training Regulations.

Prof. Dr. Saltuk Buğrahan CEYHUN

Institute Director

Aslı ıslak imzalıdır

Note: The use of original and other sources of notifications, tables, figures, and photographs in this thesis is subject to the provisions of the Law No. 5846 on Intellectual and Artistic Works.

ETHICS STATEMENT AND PLAGIARISM DECLARATION FORM

We declare that the thesis titled "Cerium Oxide Thin Film Growth Using Pulsed Electron Deposition Method" presented as a Master's thesis under the supervision of Assoc. Prof. Dr. Mustafa Tolga Yurtcan has been written in compliance with scientific ethical principles, that the sources used are cited in the bibliography, and that the similarity ratios as determined by the Turnitin program specified by the Graduate School of Natural And Applied Sciences have not been exceeded and are as indicated below.

Thesis Chapters	Thesis Similarity Ratio (%)	Maximum Ratio (%)
Introduction	24	30
Theoretical Foundation	17	30
Materials and Method	19	35
Research Findings and Discussion	17	20
Conclusion and Recommendations	7	20
Thesis as a Whole	22	25

Note: Similarities of up to seven words can be excluded from scanning for the Title, Bibliography, Table of Contents, Acknowledgements, Index, and Appendices sections. In addition to the maximum similarity rates mentioned above, the similarity ratio from any single source should not exceed 5%.

We declare and accept that the information provided is accurate, and we acknowledge that we will bear any legal responsibility that may arise otherwise.

Thesis Writer (Student)	Thesis Supervisor
Thekra ALQUTAMY	Assoc. Prof. Dr. Mustafa Tolga YURTCAN
29.8.2024	29.8.2024
İmza: Aslı ıslak imzalıdır	İmza: Aslı ıslak imzalıdır

* If there is any restriction on publishing the thesis in YÖKTEZ (the Turkish Higher Education Council's thesis database), please fill out the section below.

☐ Due to the ongoing process of patent application or patent acquisition related to the thesis, access to the thesis has been restricted for a period of 2 (two) years by the decision of the Institute Management Board dated …./…/…. and numbered …………...

☒ Due to the decision of the Institute Management Board dated …./…/…. and numbered …………, access to the thesis has been restricted for a period of 6 (six) months.

ACKNOWLEDGEMENTS

ÖZET

YÜKSEK LİSANS TEZİ

DARBELİ ELEKTRON BİRİKTİRME YÖNTEMİYLE SERYUM OKSİT İNCE FİLM BÜYÜTÜLMESİ

Thekra ALQUTAMY

Danışman: Doç. Dr. Mustafa Tolga YURTCAN

Amaç: Bu çalışma, CeO_2 ile yakın kafes uyumuna sahip $LaAlO_3$ alttaşları üzerine seryum oksit ince filmlerin büyütülmesi ve karakterizasyonunu araştırmayı amaçlamaktadır. Araştırma, optimum büyütme sıcaklığının belirlenmesi ve kataliz, biyomedikal alanlar ve mikroelektronik gibi potansiyel uygulamalar için filmlerin yüzey kalitesi ve kristallik durumunun değerlendirilmesine odaklanmaktadır.

Yöntem: Seryum oksit ince filmleri, ortam sıcaklığından 600 °C'ye kadar olan sıcaklıklarda, 100 °C artışlarla, darbeli elektron biriktirme yöntemi kullanılarak $LaAlO_3$ alttaşları üzerine biriktirilmiştir. Daha önce hazırlanmış bir CeO_2 hedef, %99.999 saf oksijen gazı ile 10 mTorr basınç altında biriktirme için kullanılmıştır. Ablasyon işlemi, 15 keV'de çalışan bir elektron kaynağı ile gerçekleştirilmiştir. Elementel analiz için X-ışını fotoelektron spektroskopisi (XPS), faz tanımlaması için düşey giriş açılı X-ışını kırınımı (GIXRD) ve yüzey karakterizasyonu için taramalı elektron mikroskobu (SEM) ve atomik kuvvet mikroskobu (AFM) gibi çeşitli analitik teknikler kullanılmıştır.

Bulgular: XPS analizi, biriktirilen filmlerde yalnızca seryum ve oksijenin varlığını doğrulamıştır. GIXRD sonuçları, numunelerin ağırlıklı olarak Ce_2O_3'e ait yüksek şiddetli tek bir pik sergilediğini ortaya koymuştur. Detaylı GIXRD analizi, CeO_2, Ce_2O_3 ve Ce_7O_{12} olmak üzere çok düşük şiddetlere sahip üç farklı seryum oksit fazının oluştuğunu göstermiştir. SEM ve AFM analizleri, 200 °C'de biriktirilen ve 15 Torr'da tavlanan numunenin, mikroelektronik ve fotonik gibi uygulamalarda cihaz verimliliğini artırmak için önemli olan en pürüzsüz yüzeye sahip olduğunu göstermiştir.

Sonuç: En iyi Ce_2O_3 kristalliğinin elde edilmesi için optimum büyüme sıcaklığı 300 °C olarak bulunmuştur. En pürüzsüz yüzey, 200 °C'de biriktirilen ve 15 Torr'da tavlanan filmler için elde edilmiştir. Buna karşılık, alttaşı hedefin normaliyle dik konumlandırmak veya 30 Torr'da tavlamak, ince filmlerin kalitesini düşürmüştür. Çalışma, nano-düz yüzeylere sahip bu seryum oksit ince filmlerin, özellikle yüksek yüzey kalitesi ve düzgünlük gerektiren çeşitli uygulamalar için uygun olduğunu sonucunu göstermektedir.

Anahtar Kelimeler: seryum oksit, CeO_2, Ce_2O_3, Ce_7O_{12}, ince film, $LaAlO_3$ (LAO), Darbeli elektron biriktirme, PED.

Ağustos 2024, 72 sayfa

ABSTRACT

MASTER'S THESIS

CERIUM OXIDE THIN FILM GROWTH USING PULSED ELECTRON DEPOSITION METHOD

Thekra ALQUTAMY

Supervisor: Assoc. Prof. Dr. Mustafa Tolga YURTCAN

Purpose:
This study aims to investigate the growth and characterization of cerium oxide thin films on $LaAlO_3$ substrates, which have a close lattice match with CeO_2. The research focuses on determining the optimal growth temperature and evaluating the surface quality and crystallinity of the films for potential applications in catalysis, biomedical fields, and microelectronics.

Method:
Thin films of cerium oxide were deposited on $LaAlO_3$ substrates using pulsed electron deposition at temperatures ranging from ambient to 600 °C, with increments of 100 °C. A CeO_2 target, previously prepared, was used for deposition in an environment of 10 mTorr pressure with 99.999% purity oxygen gas. The ablation process was driven by an electron source operating at 15 keV. Various analytical techniques were employed, including X-ray photoelectron spectroscopy (XPS) for elemental analysis, grazing incidence X-ray diffraction (GIXRD) for phase identification, and surface characterization using scanning electron microscopy (SEM) and atomic force microscopy (AFM).

Findings:
XPS analysis confirmed the presence of only cerium and oxygen in the deposited films. GIXRD results revealed that the samples predominantly exhibited a high-intensity peak corresponding to Ce_2O_3. Detailed GIXRD analysis showed the formation of three different cerium oxide phases with very low intensities: CeO_2, Ce_2O_3, and Ce_7O_{12}. SEM and AFM analyses indicated that the sample deposited at 200 °C and annealed at 15 Torr exhibited the smoothest surface, essential for reducing light scattering and improving device efficiency in applications such as microelectronics and photonics.

Results:
The optimal growth temperature for achieving the best crystallinity of Ce_2O_3 was found to be 300 °C. The smoothest surface was obtained for films deposited at 200 °C and annealed at 15 Torr. Conversely, placing the substrate perpendicular to the target's normal or annealing at 30 Torr reduced the quality of the thin films. The study concludes that these cerium oxide thin films, with their nano-smooth surfaces, are suitable for various applications, particularly in areas requiring high surface quality and uniformity.

Keywords: cerium oxide, CeO_2, Ce_2O_3, Ce_7O_{12}, thin film, $LaAlO_3$ (LAO), pulsed electron deposition, PED.

August 2024, 72 pages

TABLE OF CONTENTS

TABLE LIST

FIGURE LIST

ABBREVIATIONS

°C	**Celsius**
Å	**Angstrom**
AFM	**Atomic Force Microscopy**
Ce	**Cerium**
CeONPs	**Cerium oxide nanoparticles**
CVD	**Chemical vapor deposition**
GIXRD	**Grazing Incidence X-Ray Diffraction**
LAO	**LaAlO$_3$**
mTorr	**millitorr**
nm	**nanometer**
O	**Oxygen**
PED	**Pulsed Electron Deposition**
PLD	**Pulsed Laser Deposition**
SEM	**Scanning Electron Microscope**
XPS	**X-Ray photoelectric spectroscopy**
XRD	**X-Ray Diffraction**

INTRODUCTION

In recent years, pulsed electron deposition (PED) has gained great importance in thin film deposition. It has various names, including channeled spark discharge and pulsed plasma deposition. It is a newly invented technology that can be applied to obtain thin films that can be used in many applications and are characterized by unique properties and high quality (Liguori et al., 2019).

A thin film is a layer of material ranging in thickness from fractions of a nanometer (monolayer) to several micrometers, and deposition is a process of controlled synthesis of materials as thin films (Abegunde et al., 2019). Using PED technique, it is possible to deposit cerium oxide in the form of thin films.

Cerium oxide nanoparticles have gained attention from scientists because of the different and unique features they possess, as they possess two oxidation states between Ce^{4+} and Ce^{3+} (Xu & Qu, 2014). Cerium atoms have the ability to simply and radically change their electronic configuration to better fit their immediate surroundings. It also shows oxygen vacancies or defects in the network structure. These arise through the loss of oxygen and/or its electrons, alternating between CeO_2 and CeO_{2-x} during reduction and oxidation reactions (Gao et al., 2014).

This study aims to deposit cerium oxide in the form of thin films, determine the optimal growth temperature and study their properties for later use in various technological fields and scientific research. this study consists of five chapters. The first chapter contains general information about the study under the title Introduction. The theoretical foundations and basic information were explained in the second part. In the third section, the system and method used are explained. The fourth chapter is devoted to studying and discussing the research results, while the conclusions and recommendations are discussed in Chapter Five.

History of nanotechnology

The inventor of modern nanotechnology is physicist Richard Feynman, winner of the 1965 Nobel Prize in Physics. He first introduced the idea of atomic-level matter manipulation in a talk titled "There's Plenty of Room at the Bottom" at the 1959 American Physical Society meeting at Caltech. This innovative concept opened up new avenues for thought, and

Feynman's theories have since been validated. He is regarded as the founding father of contemporary nanotechnology because of these factors (Hulla et al., 2015).

The future of nanotechnology

Over the course of approximately fifty years, nanotechnology has emerged as the cornerstone of extraordinary industrial applications and rapid expansion. For instance, in the pharmaceutical and medical fields, nanotechnology has significantly impacted medical devices, including imaging probes, drug delivery systems, and diagnostic biosensors (Elmer & White, 2018). Nanomaterials are widely used in the canned food industry, cosmetics, and other fields to improve manufacturing, quality, and increase the shelf life of products (Higashisaka et al., 2015). Due to their antibacterial properties against germs carried by small organisms in food, zinc oxide nanoparticles with quantum dots are currently used as food sensors to assess food quality and toxicity (Sato et al., 2008).

Nanoparticles, when used as sensors, possess unique physical properties not found in bulk materials and can operate within living cells. Nanoparticle sensors have special physical properties and can have more sensitivity than traditional devices (Riu et al., 2006). Modern nanosensors rely on a variety of advanced materials, such as carbon nanotubes, quantum dots, nanoshells, and nanopores (Kaur et al., 2019). In addition, nanosensors open up an entirely new class of integrated devices that serve as the basis for "smart sensors," or sensors that can process, store, and analyze data (Han et al., 2020). Technological advances have the potential to create previously unimaginable opportunities for the use of nanosensors in a variety of industries. For example, they can be used as networks of nanorobots to monitor real-time physiological parameters in human medicine or as diagnostic and therapeutic devices at the molecular level (Devreese, 2007).

When employed for electroanalysis, nanoparticles can exhibit four distinct advantages over macroelectrodes: increased mass transport, catalysis, a large effective surface area, and control over the electrode microenvironment. As a result, a lot of research has been done on their synthesis, characterization, and use in the identification of numerous electroactive species (Welch & Compton, 2006).

The development of photocatalysis using nanotechnology is a topic that still attracts many researchers from around the world to study. A careful examination of the special properties of nanoparticles and how they are able to relate to photocatalysis is one of the recent topics. To improve the photocatalytic and/or optical properties of semiconductor materials, which are now becoming popular and receiving widespread attention for their

importance, nanoparticles are also being used. In inorganic semiconductor nanocomposites and doped, conjugated, capped, and sensitized nanocomposite systems. Electrochemical-assisted photocatalysis has been linked to the application of nanocrystalline thin films. Recently, the use of nanoparticles has been proven to provide more precise mechanistic details about the photocatalytic process and its mechanism (Fu et al., 2019).

Safety evaluation of nanomaterial's

Regretfully, there is not a universally recognized standard procedure for determining the toxicity of nanomaterials. Moreover, there are currently very few globally recognized positive controls available for research on nanomaterials. In this regard, models and techniques that have been accepted globally are required in order for regulatory agencies to assess the safety of nanomaterials. Approaches for assessing the safety of nanomaterials have been established, and efforts are still underway.

Additionally, standardized techniques have been suggested for this purpose. The National Nanotechnology Characterization Laboratory in the United States and the Nanotechnology Research Coordination Group in the United Kingdom have started to develop reference materials for nanotoxicity testing. To assess nanotoxicity, the International Coordination Alliance for Nanoenvironment, Human Health, and Safety has started creating test methods (Hulla et al., 2015).

THEORETICAL FOUNDATION

Deposition

Deposition refers to the process of layering a substance on a solid surface, atom by atom or molecule by molecule. The thickness of the deposited layers in this process varies depending on the coating technology and material used, ranging from one atom to various millimeters. The formed layer acts as a coating on a surface, changing the properties of the substrate surface depending on the application. Numerous techniques, including spin coating, spraying, plating, and vacuum deposition, can be used to apply a layer of various materials to various surfaces (Darquenne, 2020).

Vapor deposition methods

This approach is classified into two types: chemical vapor deposition (CVD) and physical vapor deposition (PVD), based on the vapor deposition procedure required:

1. **Chemical vapor deposition (CVD) method:** Also referred to as chemisorption, this technique involves subjecting suspended particles (chemical vapors) in the coating chamber to several chemical reactions, including compounding and breakdown, before the particles settle as a dense, solid layer on the desired surface. Volatile byproducts are typically produced during this coating process and are expelled from the chamber by gas flow (Creighton & Ho, 2001).

2. **The physical vapor deposition PVD method:** Also known as physisorption. During this process, the solid target material goes through a phase transition, which weakens the surface before it settles on the substrate. Physical deposition is a common method for putting a thin layer of material onto a surface. The PVD technology is divided into several divisions, depending on how the solid is turned into the vapor phase (Shahidi et al., 2015).

    a. **Thermal Evaporation Deposition:** This is one of the most basic types of physical vapor deposition technology. It involves heating the target material, with electrical current to create vapor, which is then deposited on a substrate based on variables like pressure and temperature (Vaynzof, 2020).

    b. **Pulsed Laser Deposition (PLD):** This physical vapor deposition (PVD) method uses a high-energy pulsed laser beam that is concentrated inside a vacuum chamber

4

to attack the material that has to be deposited as the target. This technique involves striking the target material's surface with a high-energy pulsed laser to ablate particulates. Subsequently, these molecules transferred onto the substrate's surface (Fujioka, 2015).

c. **Sputtering Deposition**: In this technique, the target material's molecules are stripped off and deposited on the substrate. In this, material is ejected onto a "substrate", like a silicon wafer, from a "target", which is a source. Re sputtering is the re-emission of the material that has been deposited by bombardment with ions or atoms during the deposition process. The energy distribution of sputtered atoms that are expelled from the target is broad and can reach tens of eVs (Depla et al., 2010).

d. **Electron Gun Deposition:** In this approach, a thin coating of the material is deposited by hitting it with billions of high-kinetic-energy electrons and heating it until it evaporates (Abegunde et al., 2019).

The difference between Pulsed Laser Deposition (PLD) and Pulsed Electron Deposition (PED)

Both pulsed laser and pulsed electron beams produce plasmas that decelerate in a similar way. The way energy is applied to the substance being ablated varies between the procedures, though. PED uses a strong, pulsed electric spark created by pseudospark or channelspark devices to achieve the same goal. Due to the substantially cheaper cost of the electron source than the excimer laser, which is commonly utilized in PLD, PED has a major economic advantage over PLD (Strikovski et al., 2010).

A feature shared by PLD and PED is particulate matter generation. One well-known aspect of PLD is the production of particulates, the amount and size of which depend on the target material, laser wavelength, laser fluence, ambient pressure, and target-to-substrate distance. Many other types of nanoparticles, such as germanium, silicon, platinum, gold, zinc selenite, and vanadium dioxide, have been produced using PLD. PED is expected to have applications in the synthesis of nanoparticles as well (Mathis & Christen, 2007).

Thin Film

A thin film is a layer of material whose thickness ranges from nanometers to micrometers. These films are obtained through a main process called deposition (Kaiser, 2002).

Nanoscale thin films are deposited on a substrate for many reasons, to protect the substrate, change its appearance, and change the electrical or optical properties of the substrate. Thin film deposition is an important process in various applications and industries, which refers to placing a thin layer of any material on a surface, whether it is a substrate or deposited layers. Depending on whether the deposition process is physical or chemical, the deposition method is determined as a primary criterion. For example, the back of mirrors is covered with glass coated by a thin layer of metals such as silver, aluminum, and other metals. These layers are coated by deposition processes to form a reflective surface, i.e., spray painting (Kaiser, 2002; Mirshojaeian Hosseini & Nawrocki, 2021).

Types of thin films, due to their properties

Optical: It is used to manufacture coatings that do or do not reflect light and in modern screens, solar cells, optical detectors and monitors.

Electrical or electronic: used in the manufacture of devices that include semiconductors, insulators, and conductors.

Magnetic: Usually used to make digital memory disks in computers.

Chemical: Researchers and scientists have used it to create resistance to alloys, to create high electrical conductivity, diffusion and oxidation, to protect metals from corrosion, as well as to make gas sensors and protect them from leakage. (Asha & Narain, 2020)

Mechanical: It is used to reduce elasticity (increase hardness) and adhesion and use (Franzini et al., 2000) mechanical properties at a precise and more effective level.

Thermal: It is used to create thermal insulators and inhibitors. (J. Z. Zhang, 2009)

Thin film applications

Thin film technology is a broad and important modern field that includes a wide range of applications. The potential and future applications of this technology are endless and have an impact in all industrial, biological and research sectors. For example, many applications of thin films have helped in the development of semiconductors, nano-electromechanical systems with high precision, and magnetic data storage. There are recent and more advanced future predictions for thin films that have nanostructures. Due to the rapid and dramatic development in thin film deposition techniques over the last century, there has been a wide range of technological developments in various fields such as hard coatings on devices, integrated passive devices, LEDs, for power generation such as thin-film solar cells and storage thin film batteries. It also has various applications in industry, including biosensors,

decorative coatings, plasmatic devices, photovoltaic cells, acoustic wave resonators, and batteries. (Lotz et al., 1996)

Evaluation Methods for Thin Film Properties Chemical Composition

The chemical (elemental) composition of thin films can be studied by:

1. Ion scattering techniques, such as Rutherford backscatter spectroscopy (RBS).
2. Spectroscopic techniques, such as X-ray photoelectron spectroscopy (XPS) (Franzini et al., 2000)

Structure and morphology

The crystal structure and microstructures can be described by various methods, such as X-ray diffraction (XRD) and Raman spectroscopy. The surface morphology of thin films is analyzed using several devices, the most important of which are the transmission electron microscope (TEM), the scanning electron microscope (SEM), and the atomic force microscope (AFM) (Lotz et al., 1996; Williams, 1981).

MATERIALS AND METHOD

Cerium oxide

With an atomic number of 58, cerium (Ce) is a rare earth element that is a member of the lanthanide series of the periodic table. Cerium is the most abundant of the rare earth metals with an electron configuration [Xe] $4f^1 5d^1 6s^2$ because it can exist in both the +3 (Ce^{3+} = [Xe] $4f^1 5d^0 6s^0$) and +4 (Ce^{4+} = [Xe] $4f^0 5d^0 6s^0$) oxidation states, in contrast to most other rare earth metals that typically dwell in the trivalent form (Pinto et al., 1982).

Cerium oxide can be found as Ce_2O_3 (Ce^{3+}) (Figure 1.a), which has a hexagonal structure, or as pure CeO_2 (Ce^{4+}) (Figure 1.b), which has a cubic structure (the red atoms represent oxygen and the white atoms represent cerium). It is also known by other names such as ceric oxide, cerium dioxide, ceria, or simply cerium oxide. The powder is a light yellow-white color and has the chemical formula CeO_2 (Yamamoto et al., 2005).
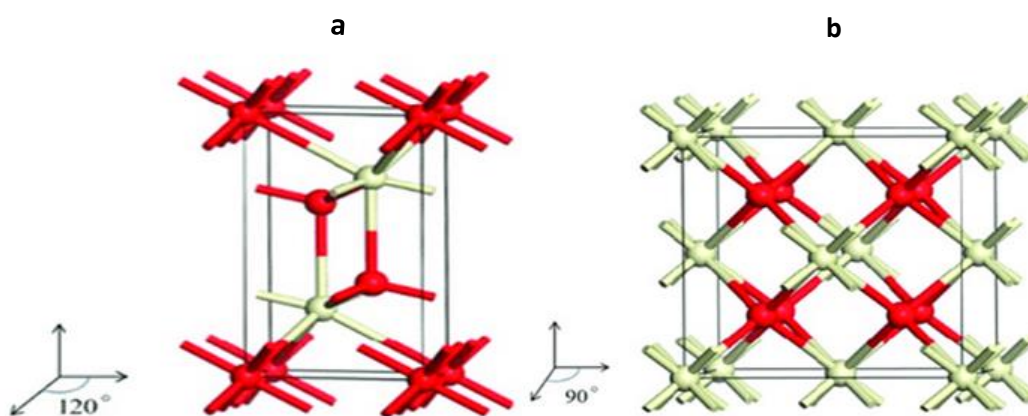
Figure 1. a) Hexagonal A-type structure of Ce_2O_3. b) The cubic (fluorite) structure of cerium dioxide (Zhou et al., 2019).

Cerium has little biological importance in mammalian physiology, although soluble Ce^{3+} salts (nitrate, acetate, chloride, etc.) have long been utilized in medicine due to their antiemetic, bacteriostatic, antibacterial, immunomodulatory, and anticancer properties. The US FDA has granted orphan drug classification to Flammacerium, a commercial dermal burn cream based on cerium nitrate. Cerium's insoluble oxide form (cerium oxide, CeO_2, or ceria) occurs naturally and is also synthesized as a bulk material and an artificial nanoparticle (NP).

Applications of Cerium oxide

Catalysis is considered one of the most important fields in which cerium oxide is used, as it acts as a catalyst for chemical reactions. For example, in catalytic converters for cars, cerium oxide reduces the emission of toxic gases by converting oxides of substances such as carbon and nitrogen and hydrocarbons into substances with less toxicity and harm. It is also used in water purification from pollutants (environmental treatment); studies have shown that it plays an important role in the delivery of medicines; and research is currently examining the possibility of treating some diseases due to its antioxidant properties (Ivanov et al., 2009).

Nanotechnology has the potential to revolutionize pharmacology by improving or creating new medicines. Cerium oxide nanoparticles (Nano ceria), well-known catalysts, have a remarkable pharmacological potential due to their antioxidant capabilities, Research in recent years has shown that it may act as an antioxidant for diseases including cancer, heart disease, and diabetes, as these diseases are known to be linked to oxidative stress. On the other hand, it has a role in protecting nerves through its ability to search for and carry reactive oxygen species (ROS) Recently, cerium oxide has been nominated to treat cancer through studying its redox properties and the production of reactive oxygen species in diseased cells, which leads to the death of cancer cells and the protection of unaffected cells. It has been used to deliver drugs and reduce side effects due to its ability to penetrate biological barriers (Ivanov et al., 2009).

It was found that the reactivity and cellular toxicity depend on the physical and chemical properties and surface changes of the nanoparticles active in oxidation and reduction processes. The scientists conducted the first experiments indicating that the cerium nanoparticles have the ability to remove ($\bullet$OH), which indicates the removal of ($\bullet$OH) from H_2O_2 present in aqueous solutions. After that, scientists revealed an experiment that in it, the cerium nanoparticles scan ($\bullet$OH) with high efficiency depending on the size of the nanoparticles and the amount of Ce^{+3} on the surface. The scientists conducted a simple light experiment using methyl violet and discovered that the increase of Ce^{+3} and the decrease of the cerium nanoparticles on the surface of the NPs, and the cerium nanoparticles became more effective in getting rid of hydroxide. It did not allow for a decrease in the visible absorption of methyl violet, and the researchers achieved something important in this experiment, which is the ability of cerium nanoparticles to reversely convert from Ce^{+3} to Ce^{+4} and their ability to clean (ROS) effectively. The scientists proposed a mechanism through which cerium nanoparticles to remove ($\bullet$OH), the first step refers to the oxidation of Ce^{+3} by ($\bullet$OH), and the

second step refers to the reduction of Ce^{+4} and the production of Ce^{+3}. (Dhall & Self, 2018; Dowding et al., 2014; Xue et al., 2011).

A. $Ce_2O_3 + 2[\bullet OH] \rightarrow 2CeO_2 + H_2O$

B. $2CeO_2$ (in presence of aqueous H+) $\rightarrow Ce_2O_3 + \frac{1}{2}O_2$

Many recent studies have shown that cerium nanoparticles can be used to protect solar cells from ultraviolet rays, as they have unique properties for absorbing ultraviolet rays. This leads to increasing the efficiency of solar cells, preventing damage, extending their life, and using them for longer periods Cerium nanoparticles can also be used to improve photocatalytic properties, and since they are characterized by the property of storing and releasing oxygen, they can reduce the recombination losses of solar cells. As they are considered a charge carrier agent and thus act as a scanner for photogenerated charge carriers (Arachi et al., 1999; Feng et al., 2019).

Pulsed electron deposition (PED) technique

PED is a deposition technique in the fields of materials science and engineering to produce thin films at nanoscales on the surface of substrates. The films that are deposited through this technique are distinguished by their unique properties and high quality. In this technique, a target material is deposited using a beam of electrons characterized by its speed and high energy. Nearly twenty years ago, the technology of pulsed electron deposition (PED) was developed to deposit thin films of metal oxides. This technology is widely used in electronics and photovoltaic cells. This technology has been applied in the biomedical field to replace joints of the feet by depositing a zirconium oxide coating on the bearing components. It is characterized by low corrosion. (Liguori et al., 2019).

This technology has features such as flexibility and its ability to control the manufacture of membranes in terms of thickness and surface smoothness by adjusting the duration and number of pulses, pressure, and temperature. Working with this technology may be hampered by several challenges, including equipment costs and the limitations of some materials that cannot be disposed of (Arisi et al., 2007).

In recent years, (PED) has become an alternative to pulsed laser deposition (PLD) as a technology for producing thin films. PED has some of the same advantages as PLD for deposition. These include: easy control of film thickness, ease of preparation, and measurement of the chemical elements of the multi-component film that is almost identical to the target material, low consumption of target materials and a relatively high deposition rate.

In addition, PED deposits materials that are transparent to UV rays and PLD fails to do so (Bleu et al., 2018).

Applications of PED technique

1. The PED technique has been recently demonstrated to be an effective method for fabricating highly-adherent and nanostructured bioactive thin films and coatings, with fine control over film composition. (Bellucci et al., 2017)

2. Dielectric films for capacitors and other electronic components are made using PED. It is possible to customize these films to have particular dielectric qualities, which are necessary to maximize the efficiency of electrical equipment. (Mazzer et al., 2016).

3. PED-deposited films find utility in a variety of sensing applications, such as chemical, bio, and gas sensors. The method enables the deposition of selective and sensitive thin films that are capable of identifying particular analysts (G. Zhang, 2013)

4. PED is used in the photovoltaic field to deposit thin films of materials that are utilized in solar cells. This covers the deposit of transparent conductive layers, buffer layers, and absorber layers. PED is a useful technology in many industrial and research applications because it can deposit high-quality films with controlled thickness, content, and microstructure in an efficient manner. (Schock, 1996).

PED principle

Electrons accelerated with a high voltage by an electron gun and directed to the target with an aluminum oxide ceramic. In order to deposit thin layers, the pulse ablates the target material, creating plasma, which then ejects perpendicular to the surface of the target. Substrate is placed facing to the target materials normal. Thin film can be formed by depositing a pulsed flow of material on a substrate, as shown in Figure 2 (Neocera, 2002).
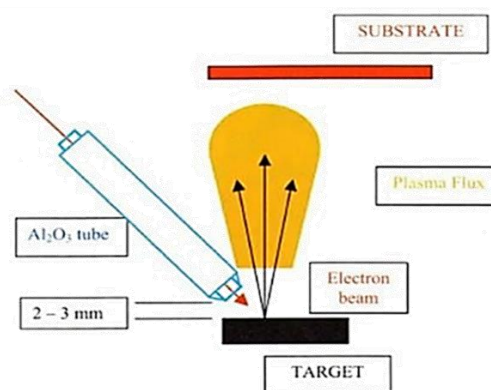
Figure 2. General scheme of PED process (Neocera, 2002).

The CeO$_2$ target preparation

To manufacture a solid target pellet, CeO$_2$ powder (MaTecK, 99.9%) was pressed in a 1″diameter die set under 12 tons of pressure and then sintered in a tube furnace (ProTherm PZF-12-50-500) at 1150 °C in an air atmosphere for two hours. Figure 3 shows the CeO$_2$ target used for depositions (Yurtcan, 2021).

Figure 3. CeO$_2$ target pellet

Substrate preparation

Lanthanum aluminate, or LaAlO$_3$, is an inorganic compound often abbreviated as LAO. It is a deformed ceramic oxide with a perovskite structure. All substrates were sliced from a <100> oriented, one-side polished, 3" diameter, 0.5mm thick LAO wafer as shown in Figure 4. Ion scattering spectroscopy and surface X-ray diffraction were used to study and analyze the surface crystals and chemical composition of the LaAlO$_3$ single crystal. This material is used as a substrate for high-quality thin film deposition (Alves et al., 2014).
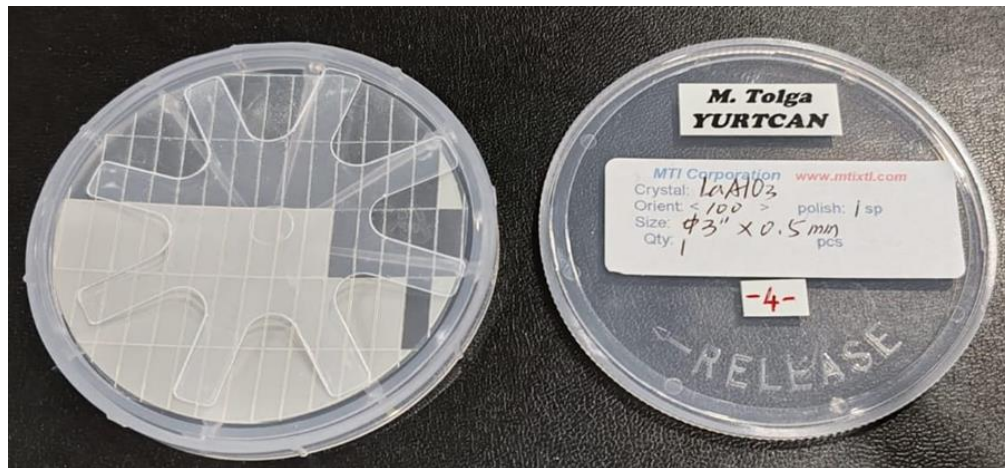
Figure 4. Sliced LAO substrates.

The substrate is cleaned before the deposition process, to ensure it is not contaminated. It was placed in an ultrasonic cleaner, as shown in Figure 5, using acetone and methanol for eight minutes each, respectively, and then dried after cleaning, the substrate was pasted on the sample holder using silver paste (Ted Pella, 200 silver paint) and then heated to 120 °C on the heating station (hot plate) 'Kaisi 818', as shown in Figure 6. To avoid contamination and remove any extraneous atoms or molecules from the deposition chamber, a pre-deposition

base pressure of 9 x 10⁻⁶ Torr was chosen. For each deposition, the target-substrate distance was fixed at 5 cm, considering the geometry of the plasma plume. The pressure was raised to 15 mTorr with high-purity oxygen (99.999%) for depositions once deposition temperatures were reached.

Figure 5. Ultrasonic Cleaner

Figure 6. Heating station (hot plate) "Kaisi 818"

PED system

PED is a powerful technology for manufacturing cost-effective high temperature superconductivity (HTS) films for coated conductor applications. The PED system is a

Neocera, Complete P180 PLD Laboratory, which has an electron gun making it possible to use as a PED system. The electron gun is a Pulsed Electron Beam Source with a 20 kV maximum energy of output electrons called PEBS-20. Figure 7 shows the system consists of three main parts: (a) vacuum system, (b) control system**.** Figure 8 shows electron gun (PEBS-20).

Figure 7. PED system (Neocera, Complete P180 PLD Laboratory) a) Vacuum system, b) Control System
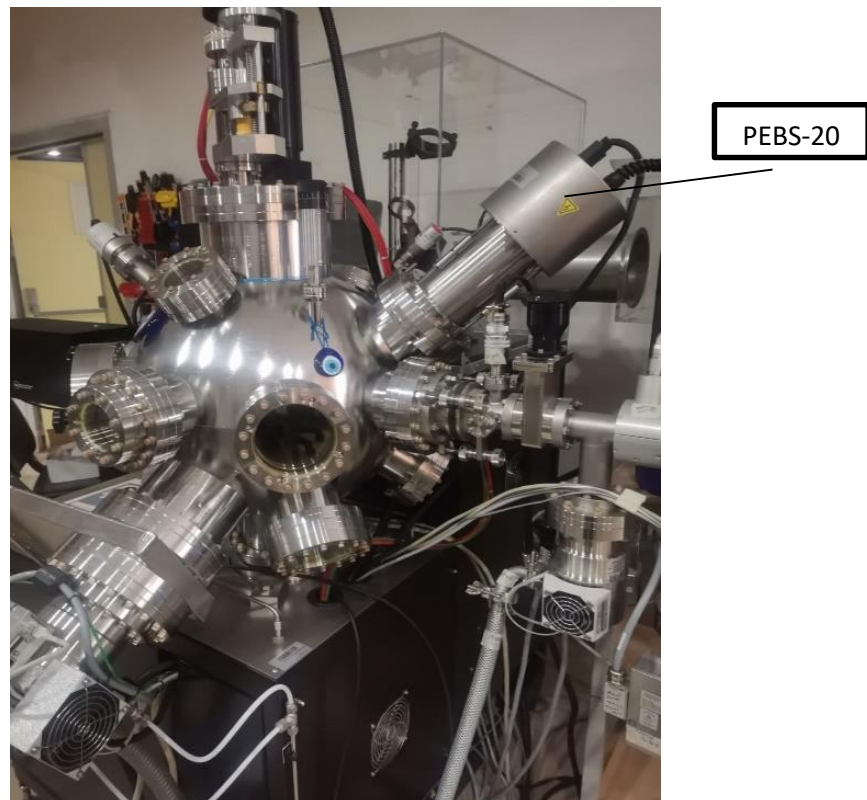
Figure 8. The electron gun (PEBS-20) of P180 PLD Laboratory

PEBS-20 requires 5 to 20 mTorr working pressures for suitable plasma formation. Table 1. Represents the specifications of the PED system.

Table 1. The Specifications of the PED System. (Neocera, 2002).

Gas pressure, oxygen	5-20 mTorr
Energy of electrons	8-20 kV
Single Pulse Energy	0.1-0.8 J
Pulse width	50-100 ns
Pulse repetition rate, max	10 Hz

At the beginning of the PED process, the cleaned substrate was placed into the vacuum chamber. To ensure the repeatability of experiments, the pre-established routines were then sequentially executed. After that, it is necessary to wait for the base pressure to reach 9×10^{-6} Torr. Once this pressure is achieved and the temperature reaches the predetermined threshold, the deposition process will commence. The temperature range for these variable values is from room temperature to 600 °C. Once the required temperature was reached, the deposition pressure was raised to 10 mTorr with high purity oxygen gas, the shield was closed, and cleaning shots were performed on the target surface. Following target cleaning, deposition was completed with 1000 shots at 1 Hz and 9000 shots at 5 Hz, and then the chamber pressure risen to 15 Torr for annealing. The system has been shut down after the cooling process is complete.

Instrumental Analysis for Thin Film Characterization

Grazing incidence X-ray diffraction (GIXRD)

In materials research, grazing incidence X-ray diffraction (GIXRD or GIXD) is a potent method for examining the structural characteristics of thin films, surfaces, and interfaces. GIXRD uses the same principle as X-ray diffraction (XRD), but with a crucial difference: the incident X-ray beam contacts the sample surface at a very shallow angle (usually less than a few degrees). This grazing incidence ensures that the X-rays only penetrate the material's surface layers, allowing the investigation of thin coatings and surface features without interference from the substrate. (Dutta, 2000). In this study, "PANalytical Empyrean XRD" was used in GIXRD mode to obtain X-ray diffraction data of samples.

Scanning electron microscope (SEM)

The scanning electron microscope is an important device in analyzing the surfaces of nano-thin films to obtain accurate images of the sample surfaces by scanning the surface with a beam of electrons that is focused on the sample surfaces, where the electrons interact with

the sample and produce secondary electrons and unique X-rays that are possible to collect and analyze to form an image that shows the topography and components of the sample surface. The most prominent components of this device are the electronic lenses, the electron source, the detectors, and the sample chamber. It is capable of producing a three-dimensional image, and the resulting images are characterized by their depth and high accuracy and provide information about the elemental composition of the sample. (Stokes, 2008)

Scanning electron microscopy (SEM) is a multipurpose technology employed in research and development as well as several industry labs these days. Materials science, including polymer science, frequently uses SEM because of its high lateral resolution, great depth of focus, and ability for X-ray microanalysis. These features help to clarify microscopic structures or distinguish between various phases to analyze the samples (Michler, 2008) "Zeiss Sigma 300" scanning electron microscope system used to obtain images of the surface topography shown in figure 9.

Figure 9. "Zeiss Sigma 300" SEM system

X-ray photoelectron spectroscopy (XPS)

Most people agree that X-ray photoelectron spectroscopy (XPS) is a crucial and significant method for characterizing and analyzing the surfaces of biological polymers. This method, also known as electron spectroscopy for chemical analysis, or ESCA, offers a complete elemental analysis of the top 10–200 Å (depending on the sample and instrumental

conditions) of any solid surface that is vacuum stable or can be made vacuum stable by cooling. It excludes hydrogen and helium. Information about chemical bonds is also given. X-ray photoelectron spectroscopy (XPS) is often considered the most quantitative, easily interpretable, and chemically informative of all currently known experimental techniques for surface research (Andrade, 1985). . The most extensively used surface analysis technique is X-ray photoelectron spectroscopy (XPS), which can be used on a wide range of materials and offers useful quantitative and chemical state information from the surface of the material under study. The characteristics of each element that leaves the sample are identified, and the peak regions can be utilized to calculate the composition of the material's surface. The initial experimental result provides a survey scan (also known as a wide scan) of the binding energy ranging from 0 to 1200 eV (Aziz & Ismail, 2017). Specs-Flex XPS system used for survey scan to determine the elemental analysis of the thin films. Conducting elemental composition analysis of the cerium oxide thin films was not possible due to the long wait time required after the experiments before the analysis could be performed.

Atomic force microscope (AFM)

Scientists and researchers specializing in the field of nanotechnology, in particular, use the atomic force microscope, which is a tool used to analyze the surfaces of nano-thin films and produce high-resolution and high-quality images by using a physical probe that allows scanning the surface of the sample. This allows obtaining details of the surface topography and its properties with high precision, and one of its most prominent components is the cantilever and the laser, photo detector, scanner, and the control system. One of the features of this tool is that it can give images of individual atoms and has the ability to give various information about magnetic and mechanical properties. There are some challenges that users of this device may face, including the small scanning size compared to the electron microscope and its slow speed, especially in high settings. In general, it is a wonderful device and tool for measuring nanoscale surfaces and helps reduce many scientific and technological challenges (Eaton & West, 2010).

SEM is better suited for imaging the composition and surface features of conductive and coated samples, as it produces high-resolution two-dimensional pictures and compositional data. AFM excels in providing three-dimensional surface profiles with atomic precision while requiring minimal sample preparation, making it appropriate for non-conductive and biological substances. Both procedures are complementary and frequently used in tandem to provide a thorough grasp of a sample's surface properties (Dubes et al., 2003). Hitachi 5100N AFM used for sample surface analysis of the thin films.

RESEARCH FINDINGS AND DISCUSSION

Grazing Incidence X-Ray Diffraction (GIXRD)

X-ray diffraction (XRD) is chosen for the analysis of thin films because it provides comprehensive information about their crystal structure and phase composition. By analyzing diffraction patterns, XRD can determine whether the film is crystalline (e.g., cubic, hexagonal), amorphous, or polycrystalline. It is also capable of identifying unwanted secondary phases, impurities, or mixed phases, and can detect even small amounts of crystalline phases within a thin film, making it an essential tool for quality control (Werzer et al., 2024). The diffraction angle (2θ) is typically scanned over a range, such as $20°$ to $80°$, though this can be adjusted based on experimental requirements.

Grazing incidence X-ray diffraction (GIXRD) is a variation of XRD specifically used for analyzing the crystallography of thin films. It is a non-destructive technique that allows for the analysis of thin films and surfaces without damaging the sample, which is particularly important for sensitive and valuable materials. GIXRD is highly sensitive to surface layers and thin films, and it minimizes the contribution of diffraction peaks from the substrate, thereby enhancing the detection of the thin film's crystal structure. The GIXRD diffraction pattern with no background subtraction or smooth data process of all the samples have one significant peak at around $53.8°$ (2θ) corresponding to hexagonal Ce_2O_3 (200). Those high intensity peaks scaled to 1000 relatively and presented through Figure 10 to Figure 16.
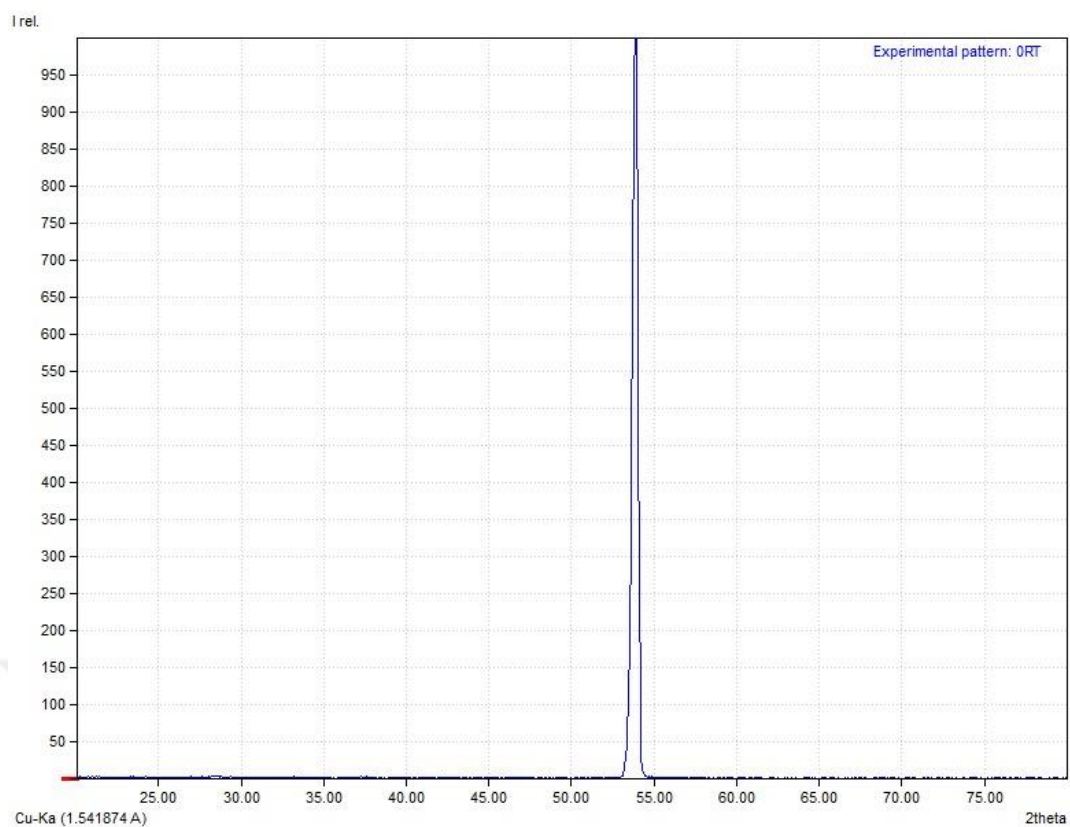
Figure 10. GIXRD of thin film deposited at 25 °C
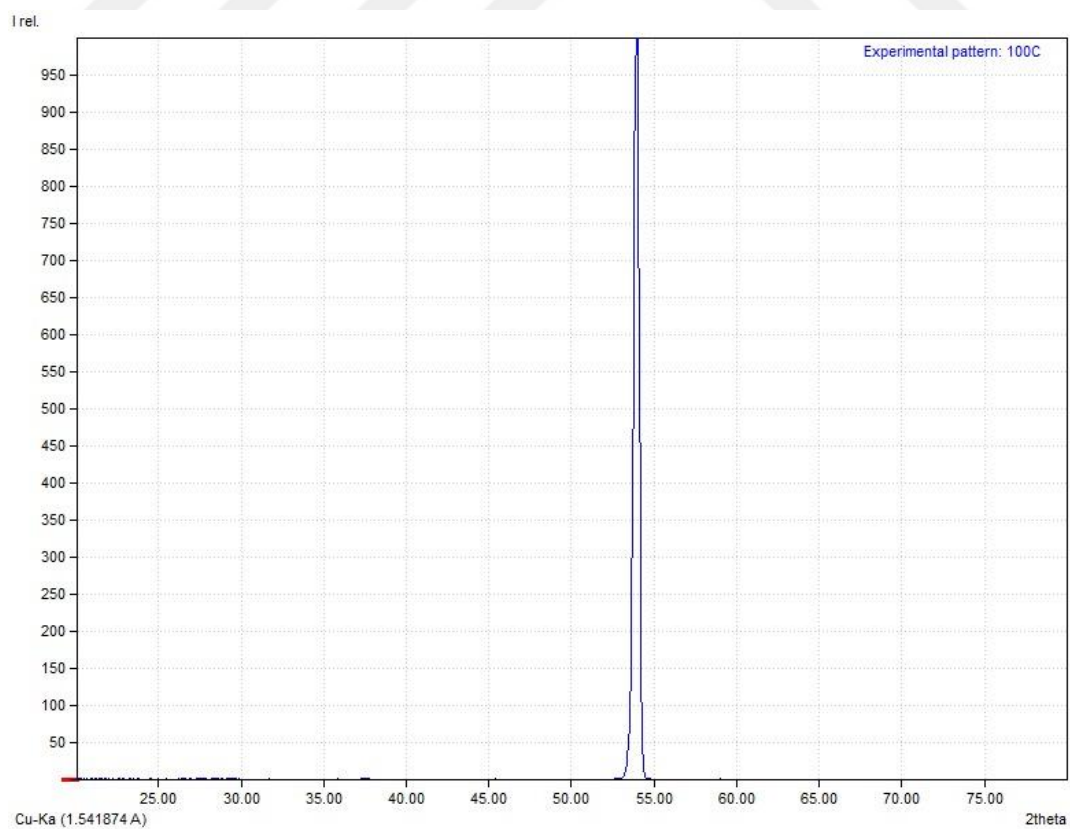
Figure 11. GIXRD of film deposited film at 100 °C

19
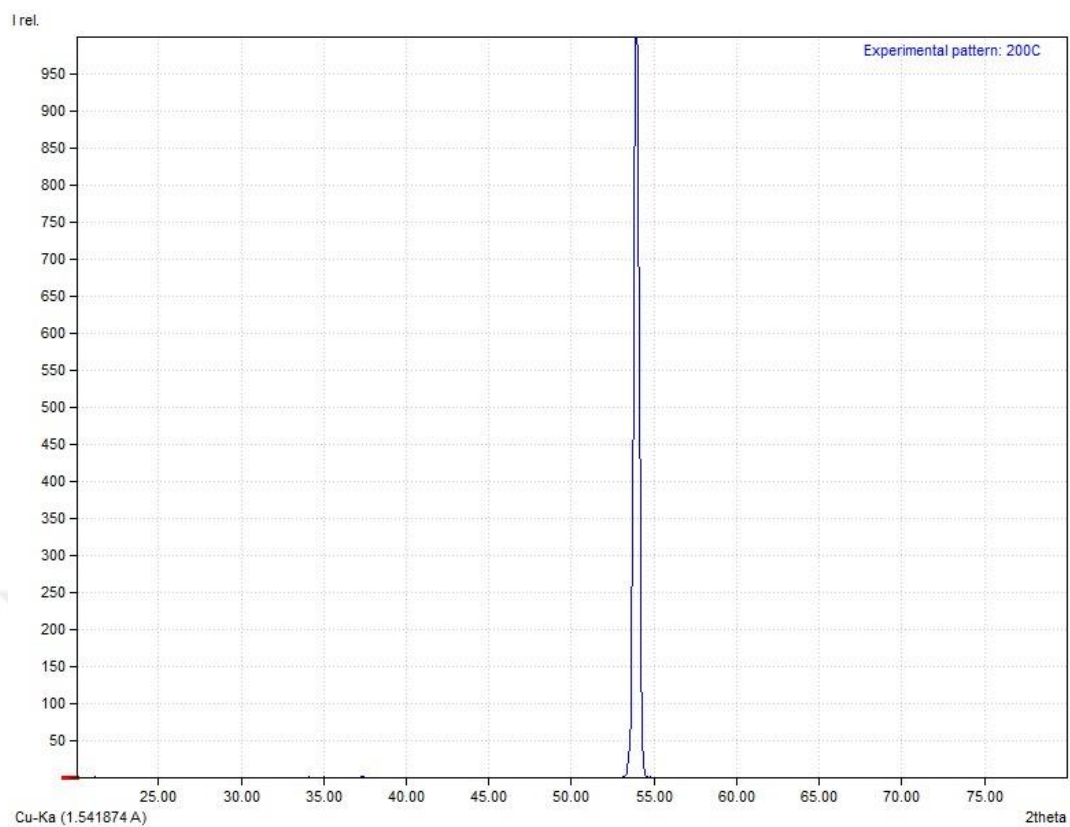
Figure 12. GIXRD of film deposited film at 200 °C

Figure 13. GIXRD of film deposited film at 300 °C
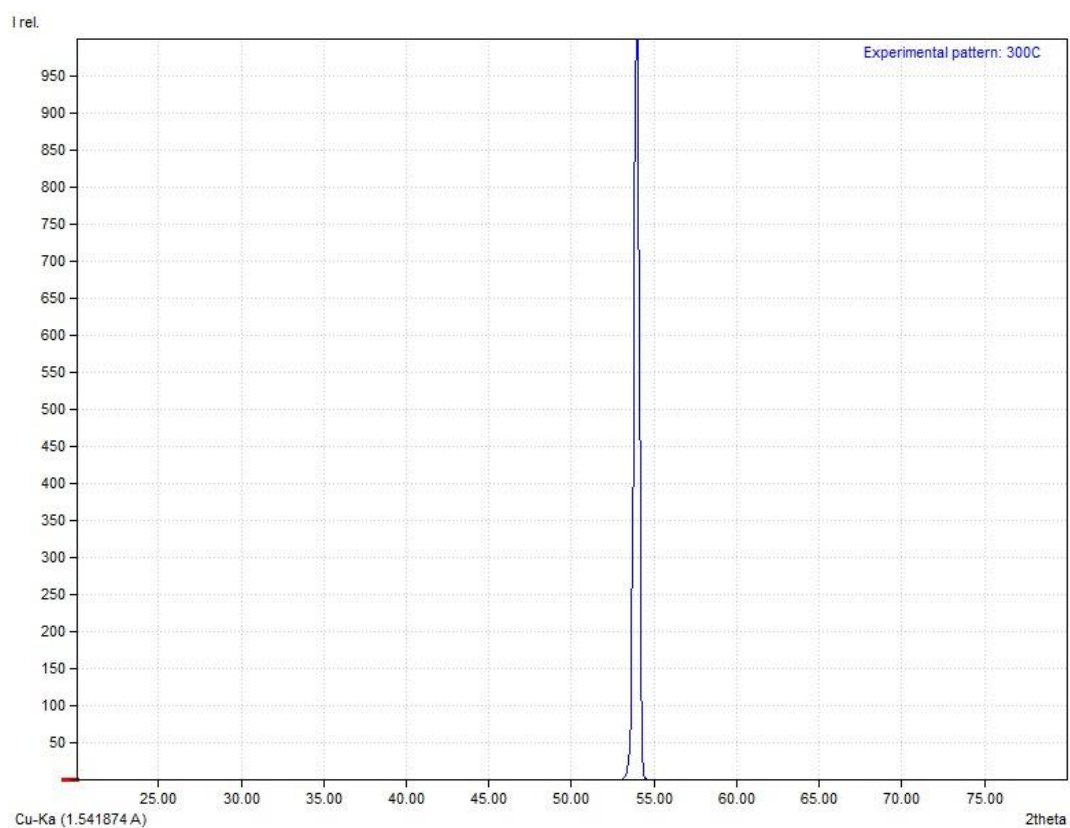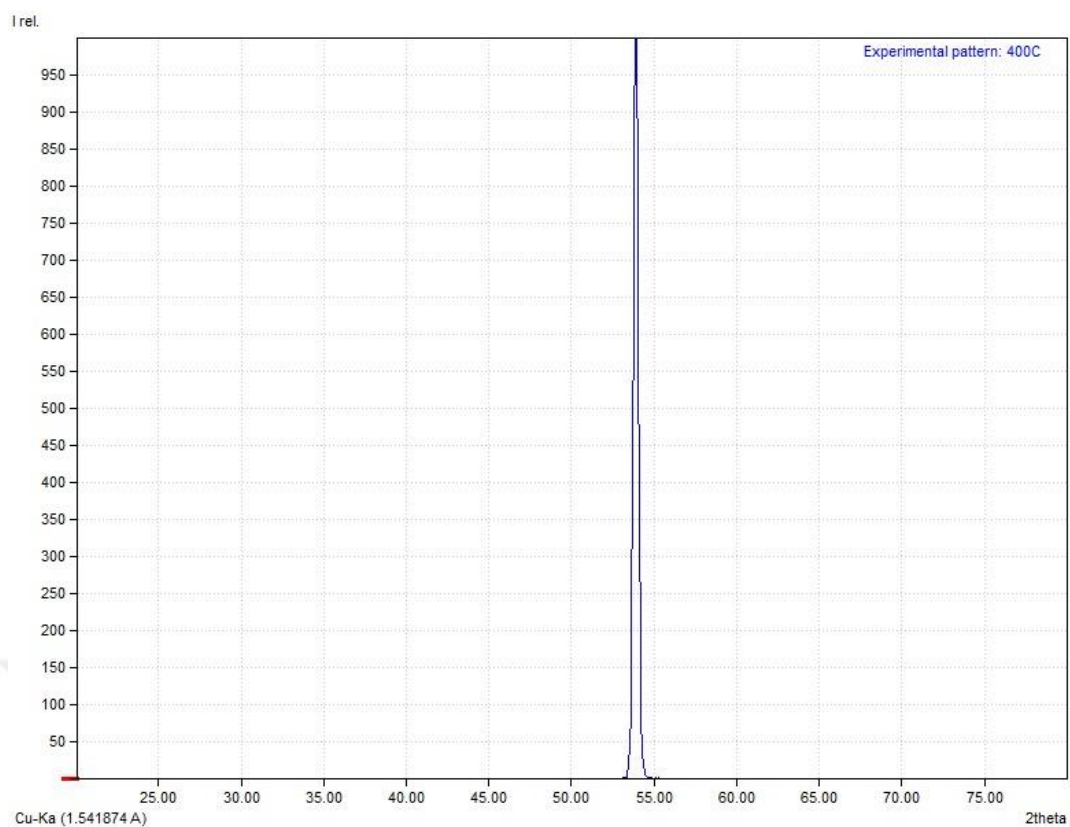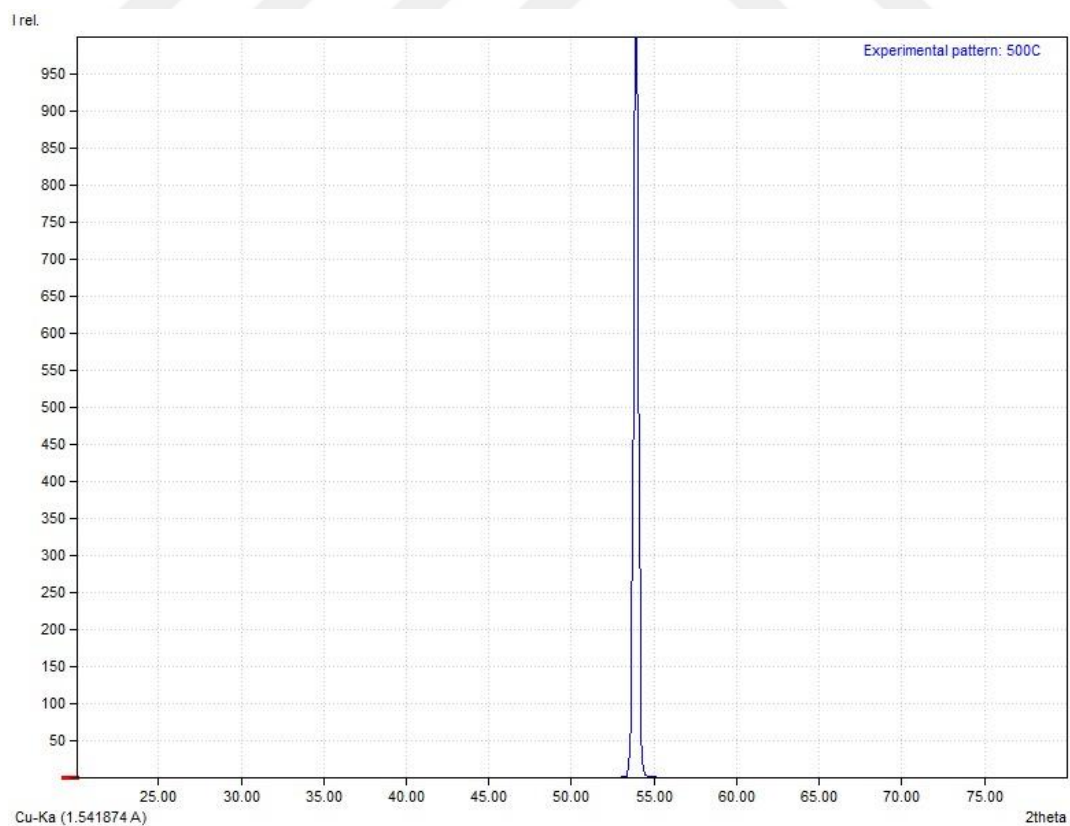
Figure 14. GIXRD of film deposited film at 400 °C.

Figure 15. GIXRD of film deposited film at 500 °C.
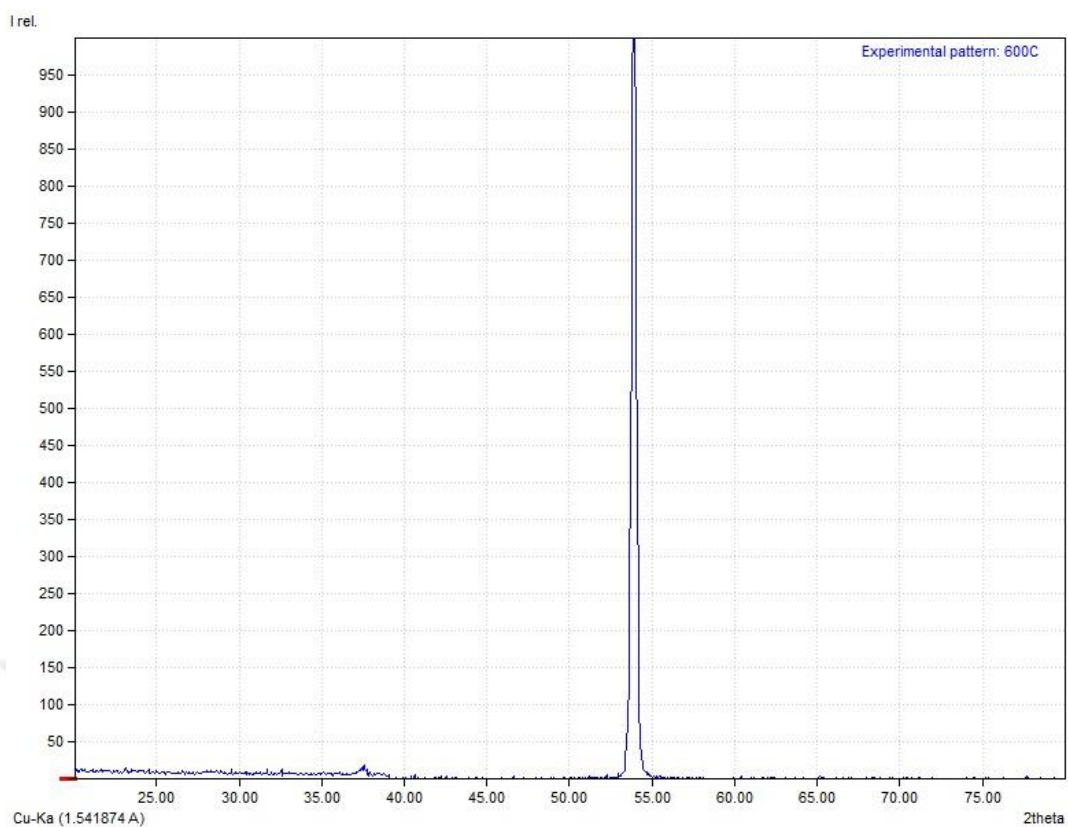
Figure 16. GIXRD of film deposited film at 600 °C.

The GIXRD diffraction pattern of all the samples are stacked and shown in Figure 17, illustrating the growth of highly crystalline cerium oxides at temperatures ranging from room temperature to 600 °C.
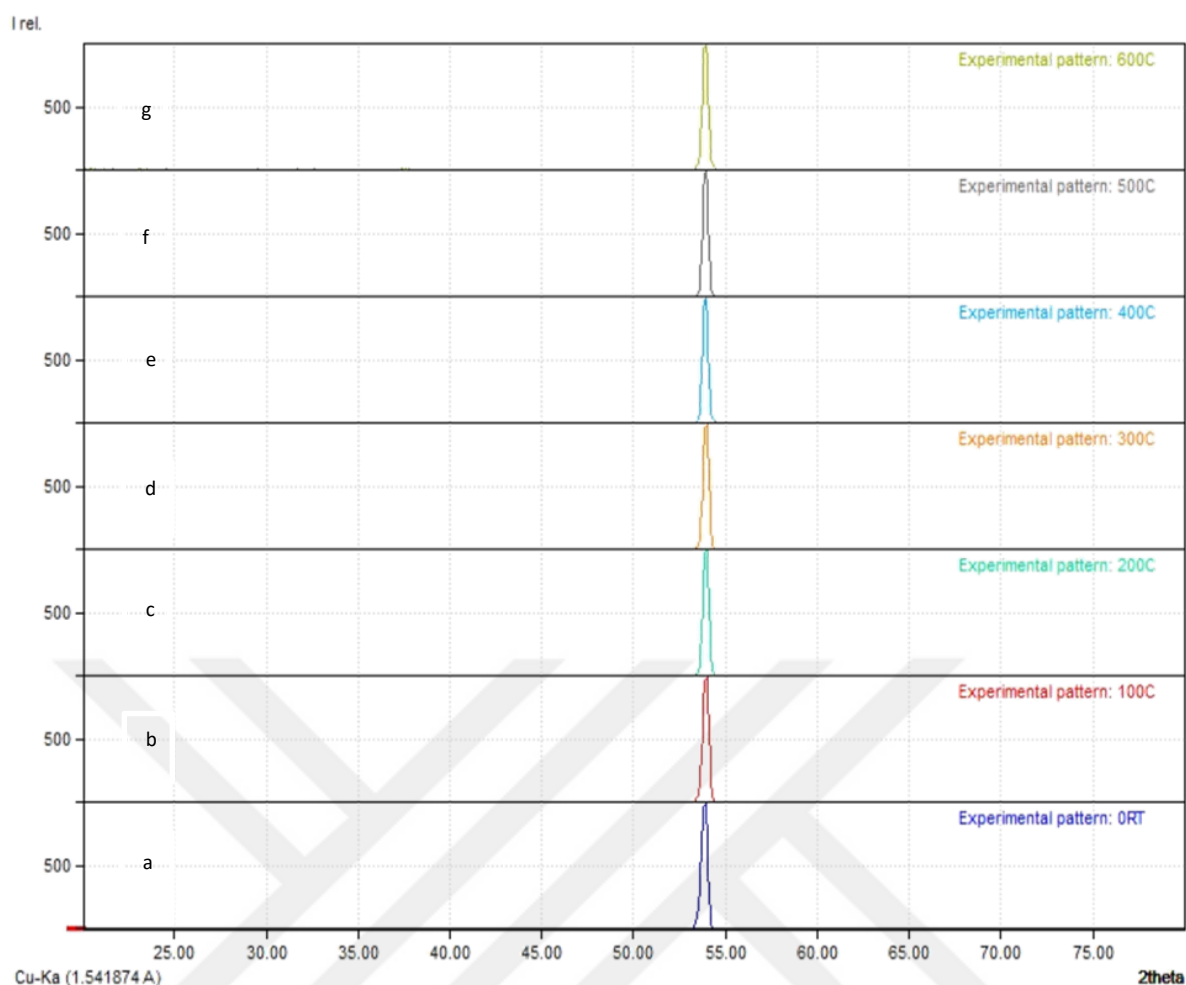
Figure 17. GIXRD of thin films deposited at **a)** 25 °C, **b)** 100 °C, **c)** 200 °C, **d)** 300 °C, **e)** 400 °C, **f)** 500 °C, and **g)** 600 °C

Since all the samples have only one high-intensity peak at the same angle, the low-intensity peaks were examined for comparison. The Open Crystallography Database (COD) was used to verify the phases of the cerium oxides, specifically CeO_2 (COD ID: 96-156-2990), Ce_2O_3 (COD ID: 96-153-1456), and Ce_7O_{12} (COD ID: 96-152-1459), which were indicated by green, red, and orange markers, respectively in Figures 18 to 26.

23
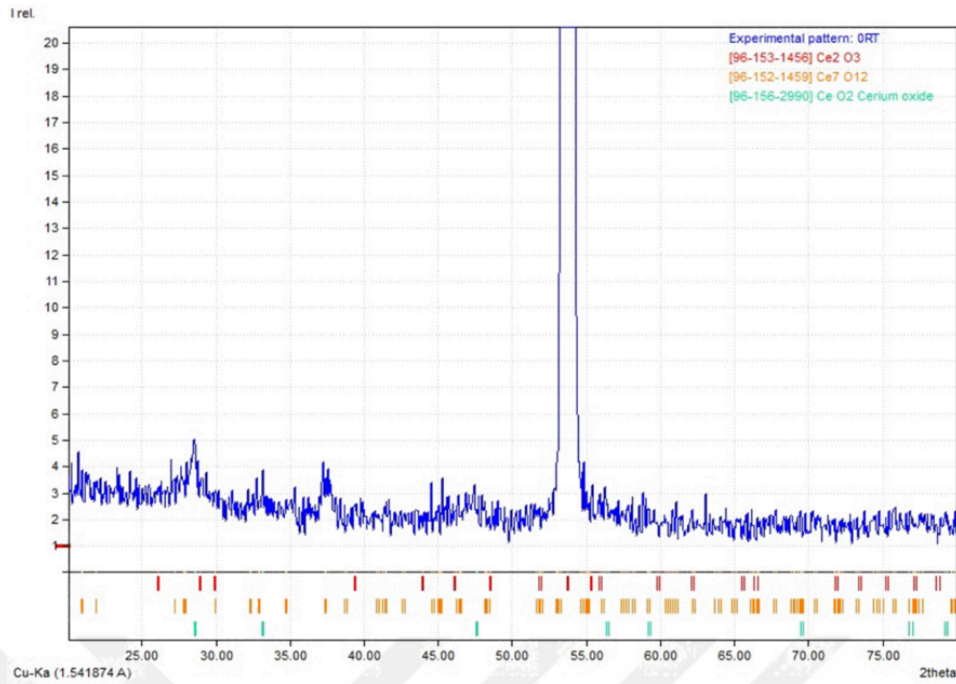
Figure 18. Low intensity GIXRD peaks of thin film deposited at 25 °C.

This sample has CeO_2 diffraction peaks at 28.54° and 33.10° corresponding to (1 1 1), (2 0 0) and Ce_7O_{12} diffraction peaks at 37.23°, 45.27° and 58.77° corresponding to (1 1 -2), (3 -2 0) and (1 -1 4).
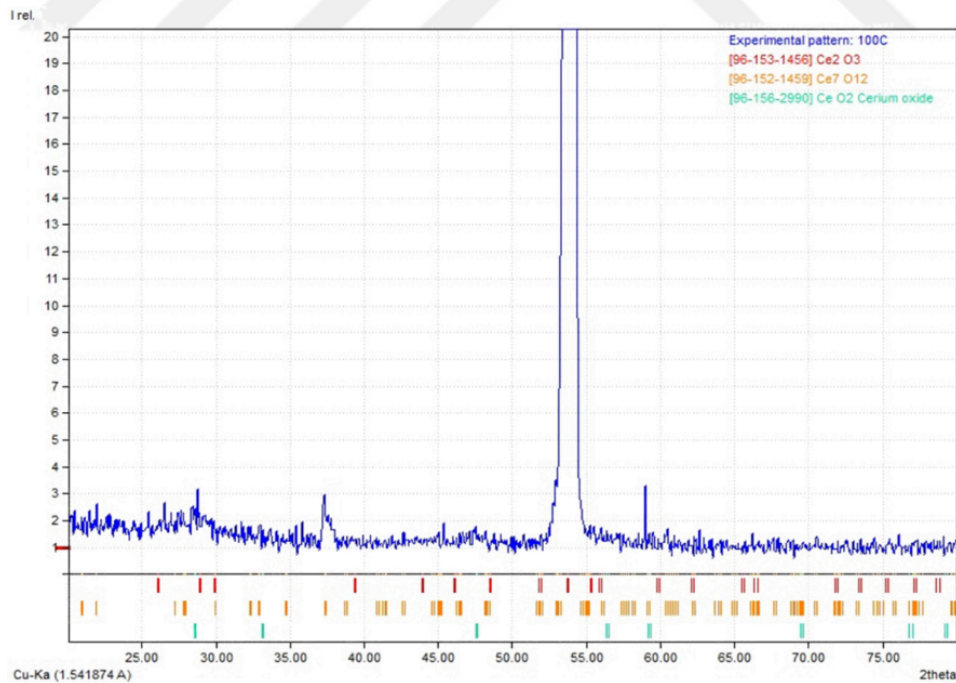
Figure 19. Low intensity GIXRD peaks of thin film deposited at 100 °C.

This sample has CeO_2 diffraction peaks at 28.71° corresponding to (1 1 1) and Ce_7O_{12} diffraction peaks at 37.30° and 58.92° corresponding to (1 2-2) and (1 -1 4) and Ce_2O_3 diffraction peaks at 28.88° corresponding to (0 0 2).

24

Figure 20. Low intensity GIXRD peaks of thin film deposited at 200 °C.

This sample has CeO_2 diffraction peaks at 76.79° corresponding to (3 1 3) and Ce_7O_{12} diffraction peaks at 37.34°, 32.32° and 76.83° corresponding to (1 2 -2), (1-1 2), (0 5 1).

Figure 21. Low intensity GIXRD peaks of thin film deposited at 300 °C.

This sample has Ce_2O_3 diffraction peaks at 48.61° corresponding to (1 1 1) and Ce_7O_{12} diffraction peaks at 37.39°,44.62°and 61.18°diffraction peak corresponding to (1 2 -2), (2 -2 2), (1 -2 4).

Figure 22. Low intensity GIXRD peaks of thin film deposited at 400 °C.

This sample has CeO_2 diffraction peaks at 59.28° corresponding to (2 2 2) and Ce_7O_{12} diffraction peaks at 37.46° and 59.28° corresponding to (1 2 -2), (1 -1 4) and Ce_2O_3 diffraction peaks at 28.85°, 48.54° corresponding to (0 0 2), (1 1 1).
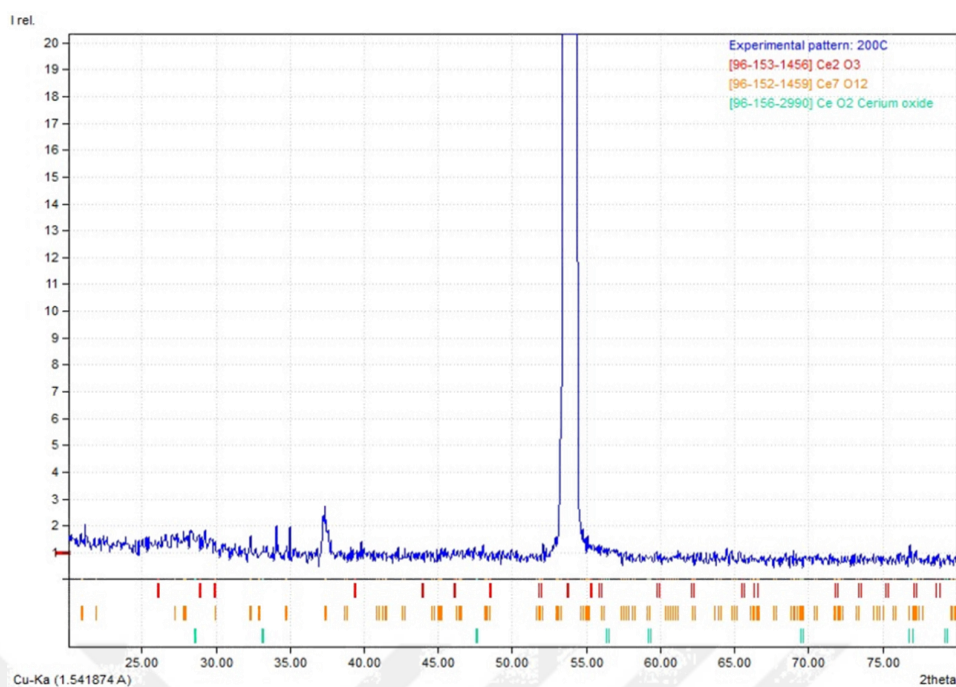

Figure 23. Low intensity GIXRD peaks of thin film deposited at 500 °C.

This sample has Ce_2O_3 diffraction peaks at 28.03° corresponding to (1 0 0) and Ce_7O_{12} diffraction peaks at 37.55° and 67.63° corresponding to (1 2 -2), (2 -2 4).
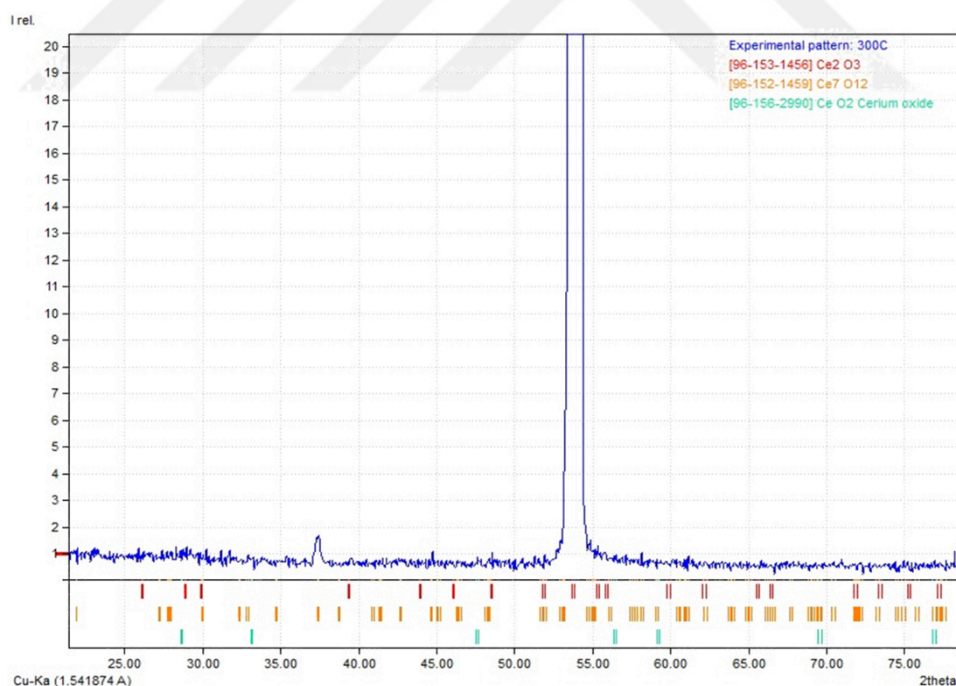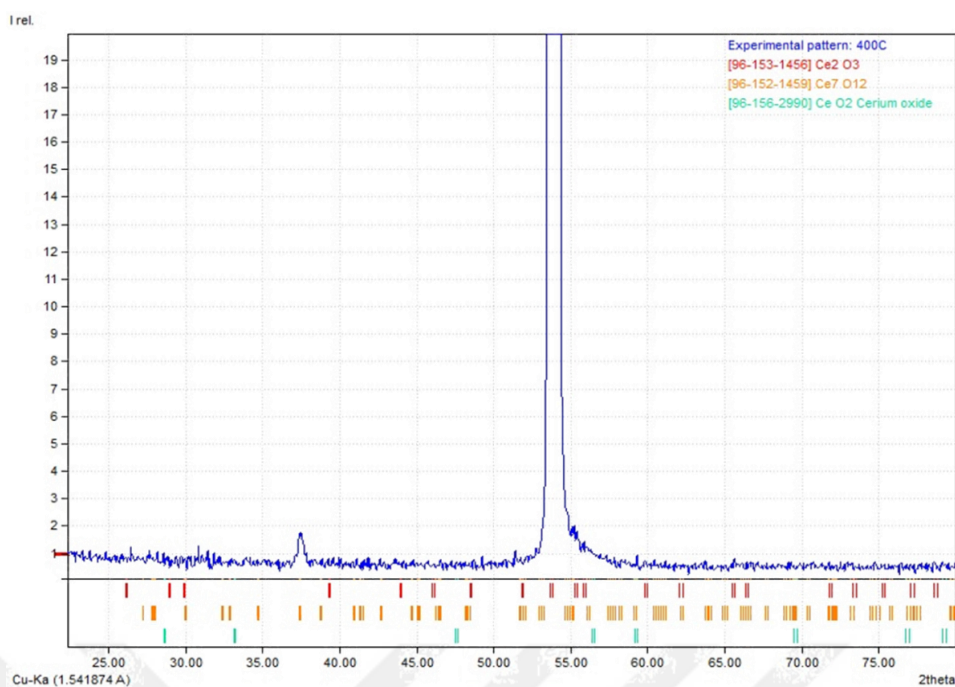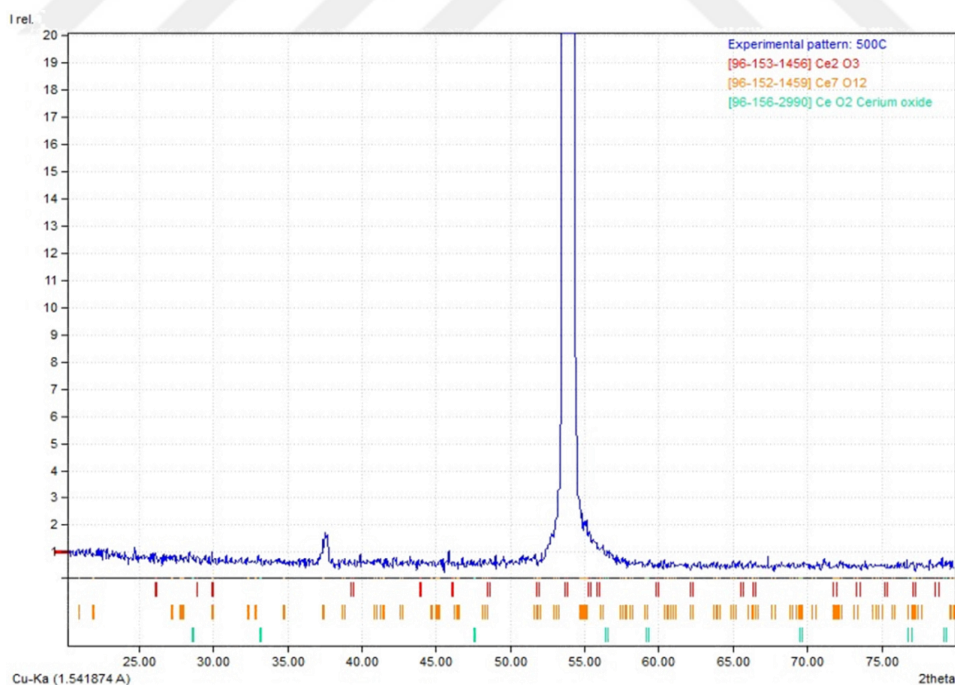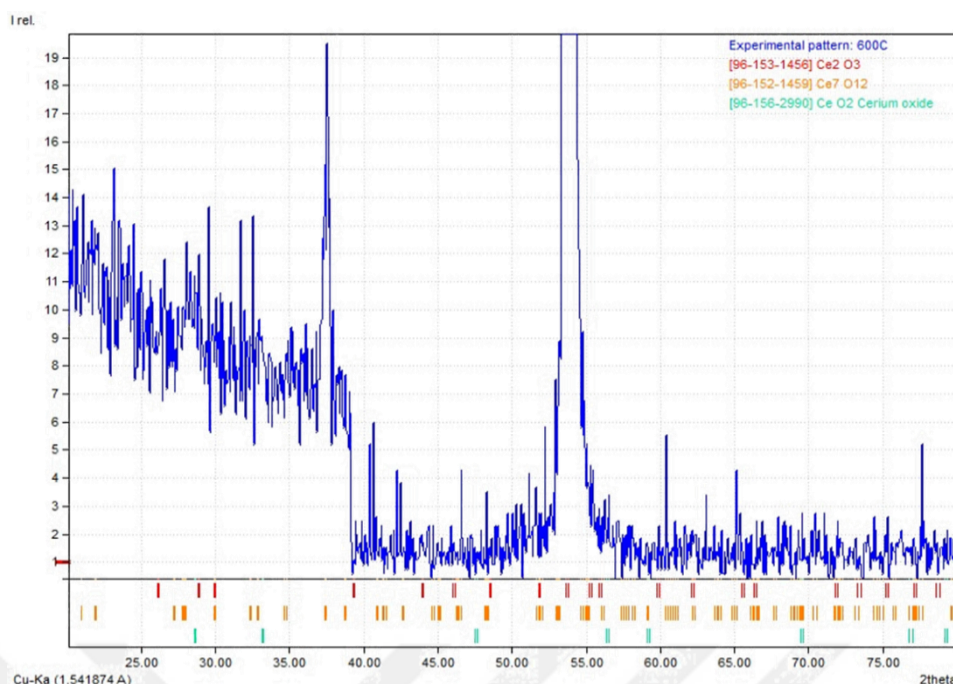
Figure 24. Low intensity GIXRD peaks of thin film deposited at 600 °C.

This sample has CeO_2 diffraction peaks at 33.51° corresponding to (2 0 0) and Ce_7O_{12} diffraction peaks at 37.50°, 60.38° and 65.14° corresponding to (1 2 1), (2 1 3), (3 1 -4) and Ce_2O_3 diffraction peaks at 26.36°, 28.83° and 65.74 corresponding to (1 0 0), (0 0 2), (1 1 3). The noise in the beginning of the analysis is not significant because background reduction is not applied for all of the samples. However, the GIXRD result is not as clean as low temperature depositions.

In order to see the effect of substrate placement orientation, a new substrate was placed perpendicular to the target at 200 °C. Placing the substrate perpendicular had no significant effect; however, different crystal orientations increased as a result of this placement. Figure 25.a and Figure 25.b shows the GIXRD analysis of the thin films deposited at 200 °C perpendicular and normal placements, respectfully.

The thin film prepared at 500°C was annealed at a higher pressure of 30 Torr to observe the effect of annealing on the thin film. Figures 26.a and 26.b show the GIXRD results of the thin film deposited at 500 °C and annealed at 30 Torr and 15 Torr, respectively.
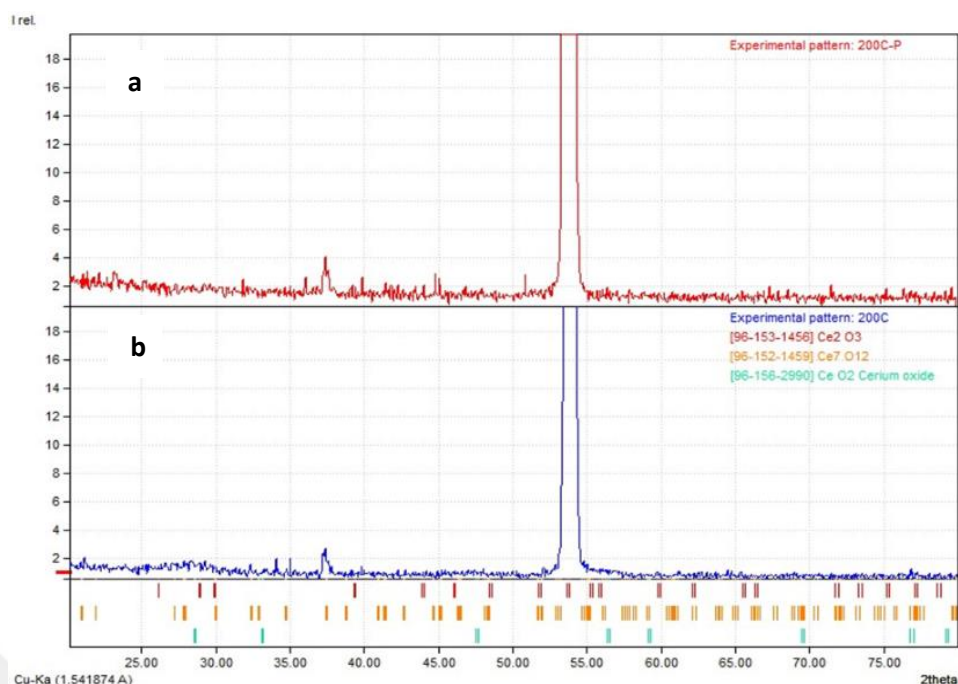
Figure 25. a) GIXRD of thin film deposited perpendicular position at 200 °C. **b)** GIXRD of thin film deposited at 200 °C.

The sample in Figure 25.a has Ce_7O_{12} diffraction peaks at 37.33°, 44.72°, 45.07° and 67.89° corresponding to (1 2 -2), (2 -2 2), (1 -1 3), (2 -2 4) and Ce_2O_3 diffraction peaks at 39.33°, 65.45° and 75.15° corresponding to (0 1 2), (1 1 3), (1 2 1) and CeO_2 diffraction peaks at 56.37° corresponding to (3 1 1).
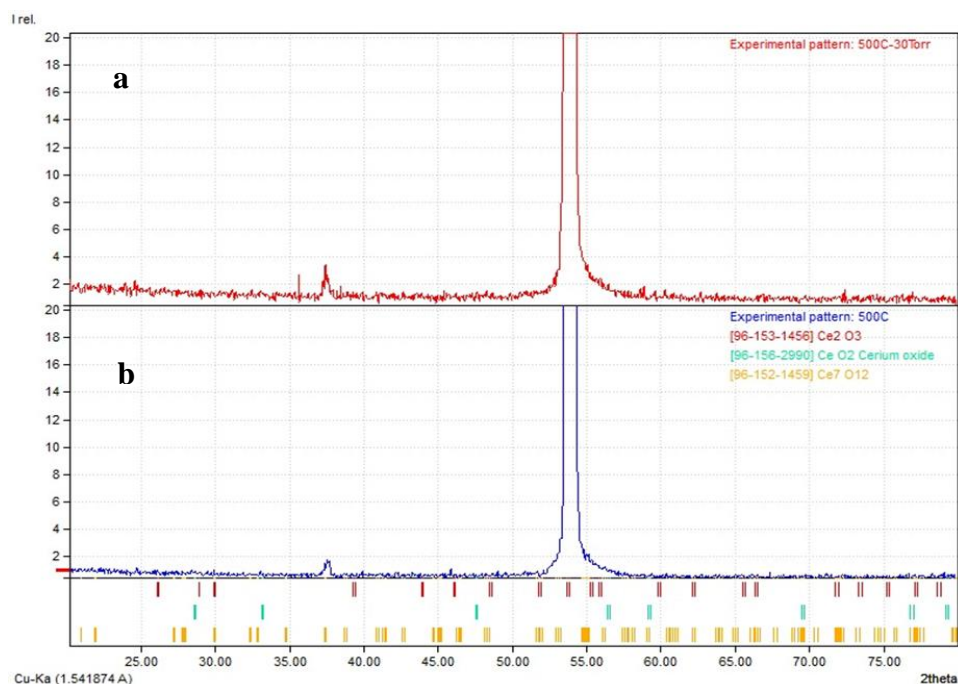
Figure 26. a) GIXRD of thin film deposited at 500 °C and annealed at 30 Torr. **b)** GIXRD of thin film deposited at 500 °C and annealed at 15 Torr.

Although both samples have low-intensity peaks in Figure 26, the peak intensity increases at higher annealing pressures, and an unidentified foreign peak is observed at 35.64°. Ce_7O_{12} diffraction peaks at 37.42°, 47.95°and 72.41° corresponding to (1 1 -2) (-2 5 0) (2 0 2). Annealing at higher pressure resulted in impurities, which is why lower annealing pressure is preferable.

Comparison of the GIXRD results revealed that the best samples in terms of crystallinity are those grown at 300 °C, 400 °C, and 500 °C. However, considering the peak corresponding to Ce_7O_{12} at 55°, the best sample was chosen to be the one grown at 300 °C. By looking at the results, it was concluded that all the samples except for sample prepared at 600 °C are background noise free and the peaks are clean (Andrle et al., 2021; Hoshino et al., 2024).

Pulsed Electron Deposition (PED) of Ce_2O_3 is not presented in the literature due to the challenges associated with maintaining the +3 oxidation state. Maintaining this oxidation state during deposition can be difficult. In this study, GIXRD analysis suggest that Ce_2O_3 was deposited as a single crystal, which is noteworthy because Ce_2O_3 has not been previously deposited using the PED method. Single-crystal Ce_2O_3 has important applications, particularly in oxygen storage, fuel cells, and sensors. The ability of Ce_2O_3 to easily switch between Ce^{3+} and Ce^{4+} states further enhances its potential in various applications (Gupta et al., 2016; Inbaraj & Chen, 2020).

Atomic Force Microscopy Results

An AFM instrument was used to evaluate the surface characteristics of thin films produced through pulsed electron deposition. Three-dimensional, two-dimensional, and linear pictures were obtained at various layers of the thin films. When the AFM pictures of the films were analyzed, the average roughness values varied dramatically depending on the degree of heat. The resolution was assessed for each thin film at each temperature using a 2-micron scale. The surface height of the sample was measured at three different distances. It is shown in the chart in red, blue and green. The values at the bottom of each image indicate the roughness values at each surface, respectively (Figure 27-35).
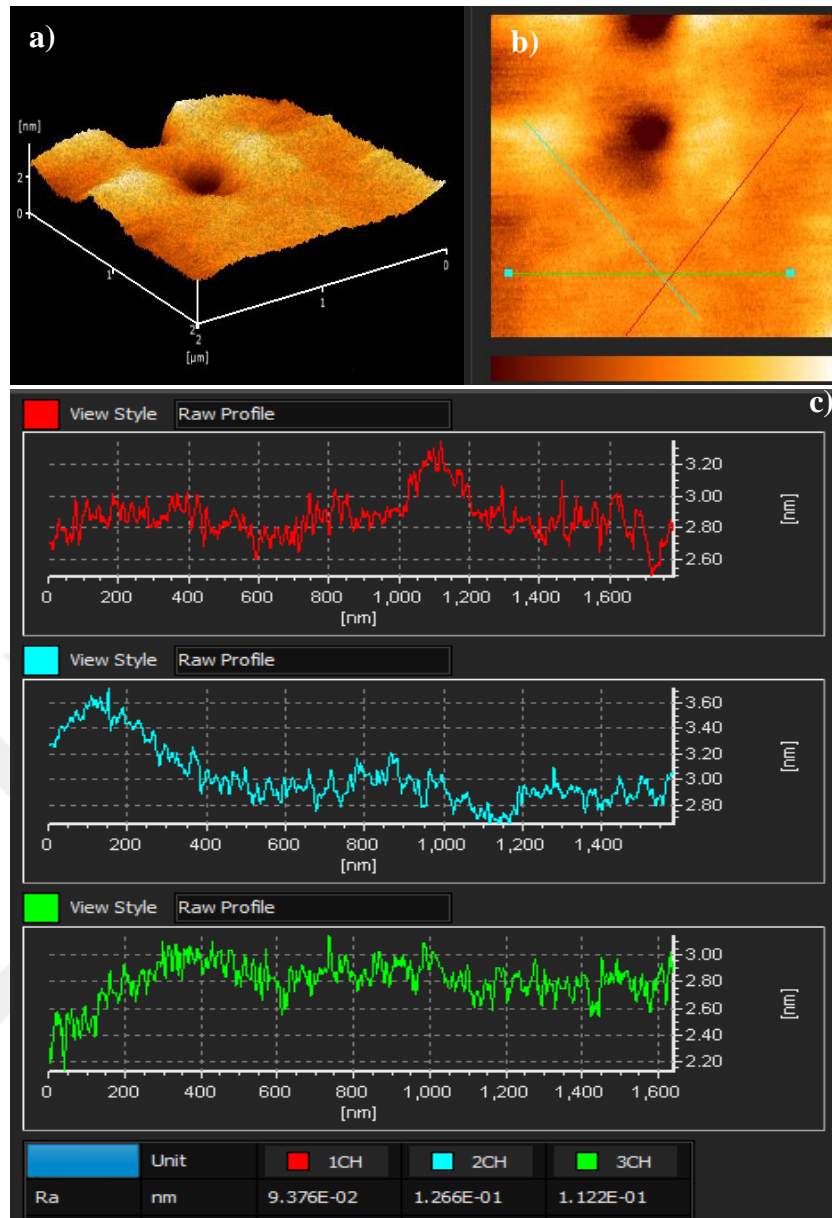
Figure 27. The AFM image of the sample surface deposited at 25 °C.

Figure 27.a shows a three-dimensional image in the plane 2 μm × 2 μm and Figure 27.b shows a two-dimensional in the plane 2 μm × 2 μm and Figure 27.c shows linear elevation AFM line height of the sample. Through the reference line, through the red line, the particle height is 3.30 nm and the roughness is 9.376×10^{-2} nm, the blue line has a particle height of 3.70 nm and the roughness is 1.266×10^{-1} nm, and through the green line it has a particle height of 3.40 nm and a roughness of 1.122×10^{-1} nm, Figure 27.a shows that the surface contains a gap indicating the beginning of the growth of nanoparticles and the growth of others with slight roughness, at a height of 2 nanometers
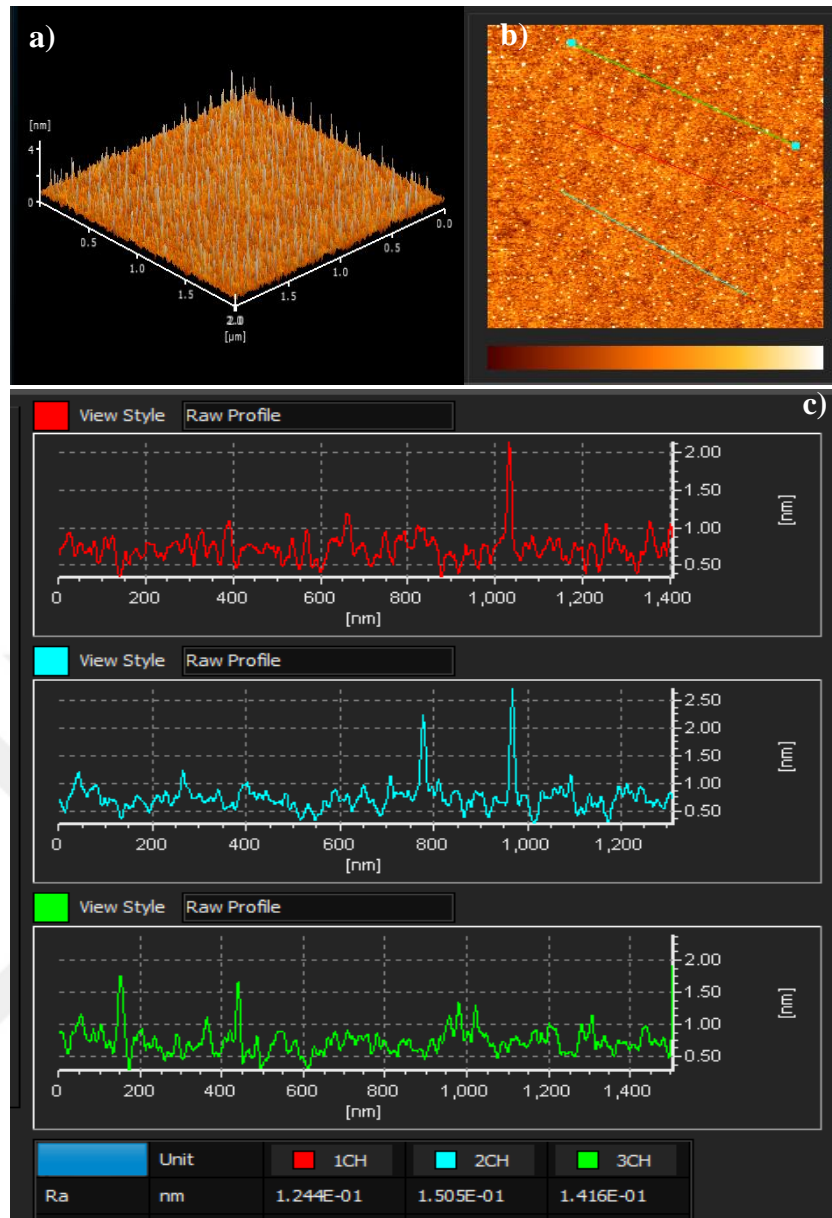
Figure 28. The AFM image of the sample surface deposited at 100 °C.

Figure 28.a shows a three-dimensional image in the plane 2 μm × 2 μm and Figure 28.b shows a two-dimensional in the plane 2 μm × 2 μm and Figure 28.c shows linear elevation AFM line height of the sample. Through the reference line, through the red line, the particle height is 2.1 nm and the roughness is 1.244×10^{-1} nm, the blue line has a particle height of 2.7 nm and the roughness is 1.505×10^{-1} nm, and through the green line it has a particle height of 1.9 nm and a roughness of 1.416×10^{-1} nm, Figure 28.a shows the growth of a large number of nanoparticles on the whole surface with higher roughness compared to the growth of the samples at previous room temperature and at a height of 4 nm.
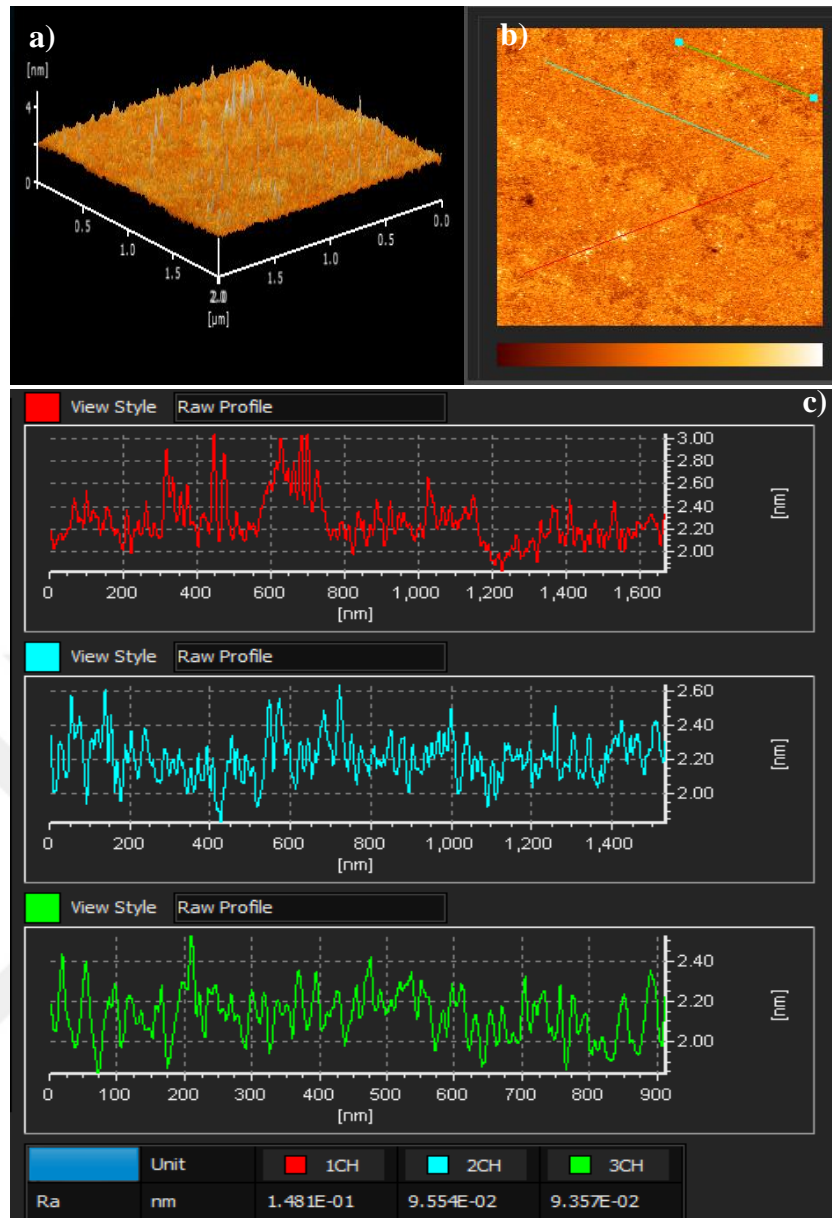
Figure 29. The AFM image of the sample surface deposited at 200 °C.

Figure 29.a shows a three-dimensional image in the plane 2 μm × 2 μm and Figure 29.b shows a two-dimensional in the plane 2 μm × 2 μm and Figure 29.c shows linear elevation AFM line height of the sample. Through the reference line, through the red line, the particle height is 3 nm and the roughness is 1.481×10^{-1} nm, the blue line has a particle height of 2.61 nm and the roughness is 9.554×10^{-2} nm, and through the green line it has a particle height of 3.60 nm and a roughness of 9.357×10^{-2} nm, Figure 29.a shows a decline in the growth of the particles and a slight growth at a height of 4 nm, The growth area of the particles indicated by the red line in image (b) shows the highest surface roughness present on the surface (a).
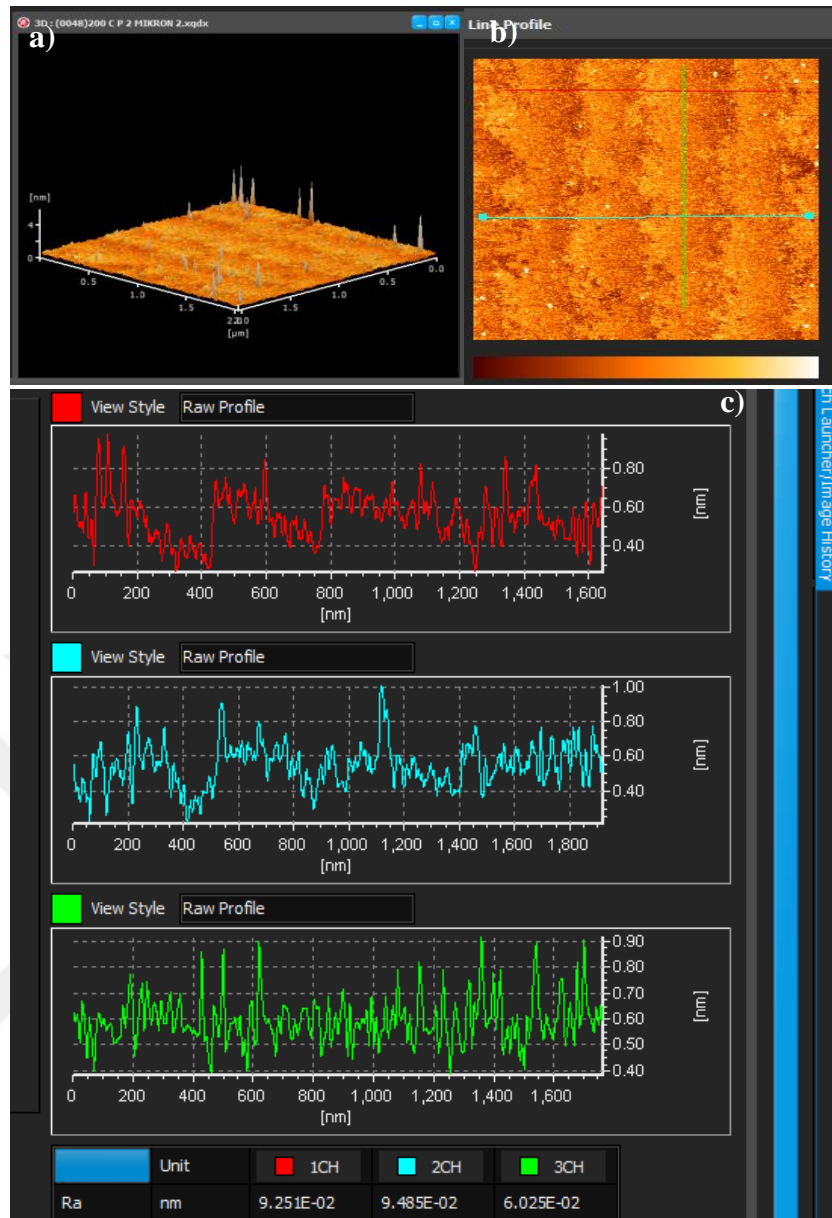
Figure 30. The AFM image of the sample surface deposited perpendicular at 200 °C

Figure 30.a shows a three-dimensional image in the plane 2 μm × 2 μm and Figure 30.b shows a two-dimensional in the plane 2 μm × 2 μm and Figure 30.c shows linear elevation AFM line height of the sample. Through the reference line, through the red line, the particle height is 0.95 nm and the roughness is 9.251×10^{-2} nm, the blue line has a particle height of 1.00 nm and the roughness is 9.489×10^{-2} nm, and through the green line it has a particle height of 0.90 nm and a roughness of 6.025×10^{-2} nm. Figure 30.a shows the growth of some particles in separate places on the surface of the substrate at a height of more than 4 nanometers. The roughness values are the lowest among all samples at all temperatures. This may be due to deposition occurring directly on the edges due to the perpendicular position of the sample.

Figure 31. The AFM image of the sample surface deposited at 300 °C

Figure 31.a shows a three-dimensional image in the plane 2 μm × 2 μm and Figure 31.b shows a two-dimensional in the plane 2 μm × 2 μm and Figure 31.c shows linear elevation AFM line height of the sample. Through the reference line, through the red line, the particle height is 2.30 nm and the roughness is 1.015×10^{-1} nm, the blue line has a particle height of 4.3 nm and the roughness is 4.986×10^{-1} nm, and through the green line it has a particle height of 2.80 nm and a roughness of 1.207×10^{-1} nm, Figure 31.a shows growth of some particles at a height of 5 nanometers and a slight increase in roughness in most of the surface.
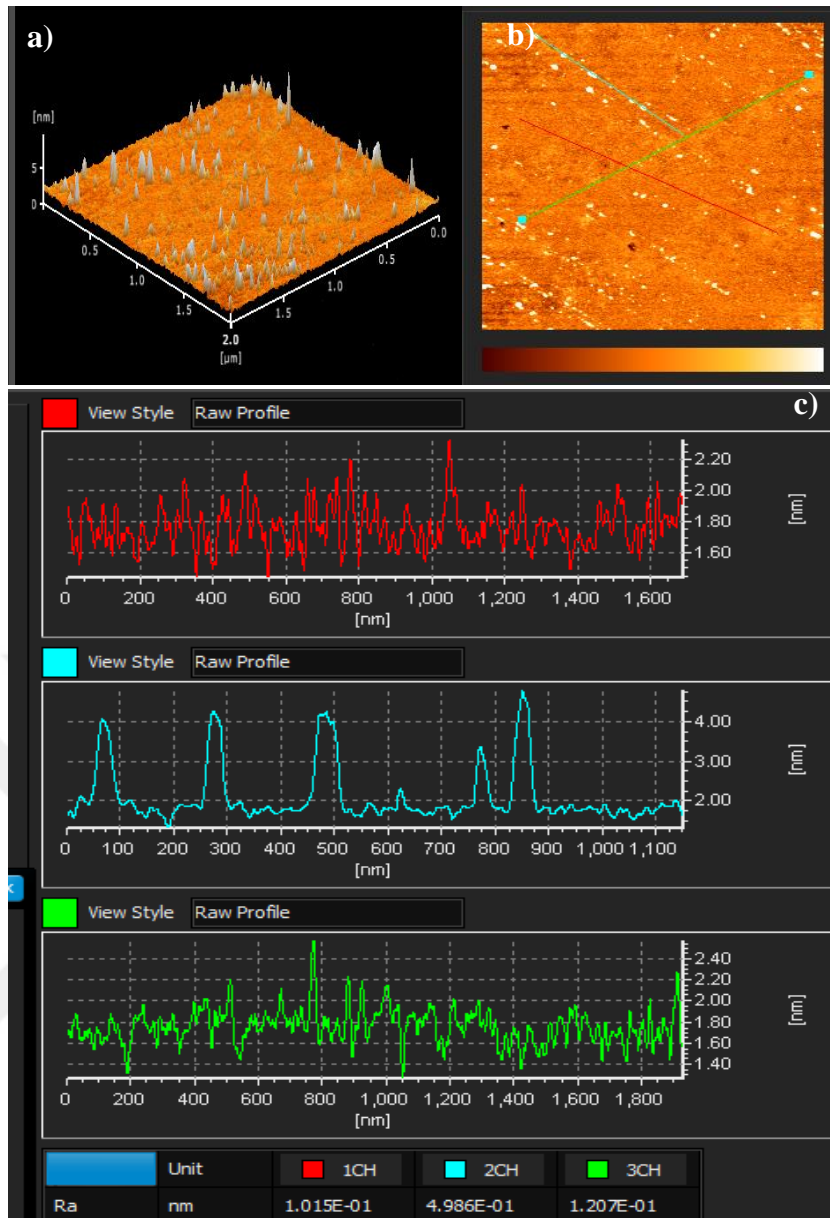
Figure 32. The AFM image of the sample surface deposited at 400 °C

Figure 32.a shows a three-dimensional image in the plane 2 μm × 2 μm and Figure 32.b shows a two-dimensional in the plane 2 μm × 2 μm and Figure 32.c shows linear elevation AFM line height of the sample. Through the reference line, through the red line, the particle height is 2.50 nm and the roughness is 1.278×10^{-1} nm, the blue line has a particle height of 2.40 nm and the roughness is 1.260×10^{-1} nm, and through the green line it has a particle height of 2.60 nm and a roughness of 1.239×10^{-1} nm, Figure 32.a shows a regular growth of particles at close heights of up to 5 nanometer. The surface is considered one of the roughest surfaces.
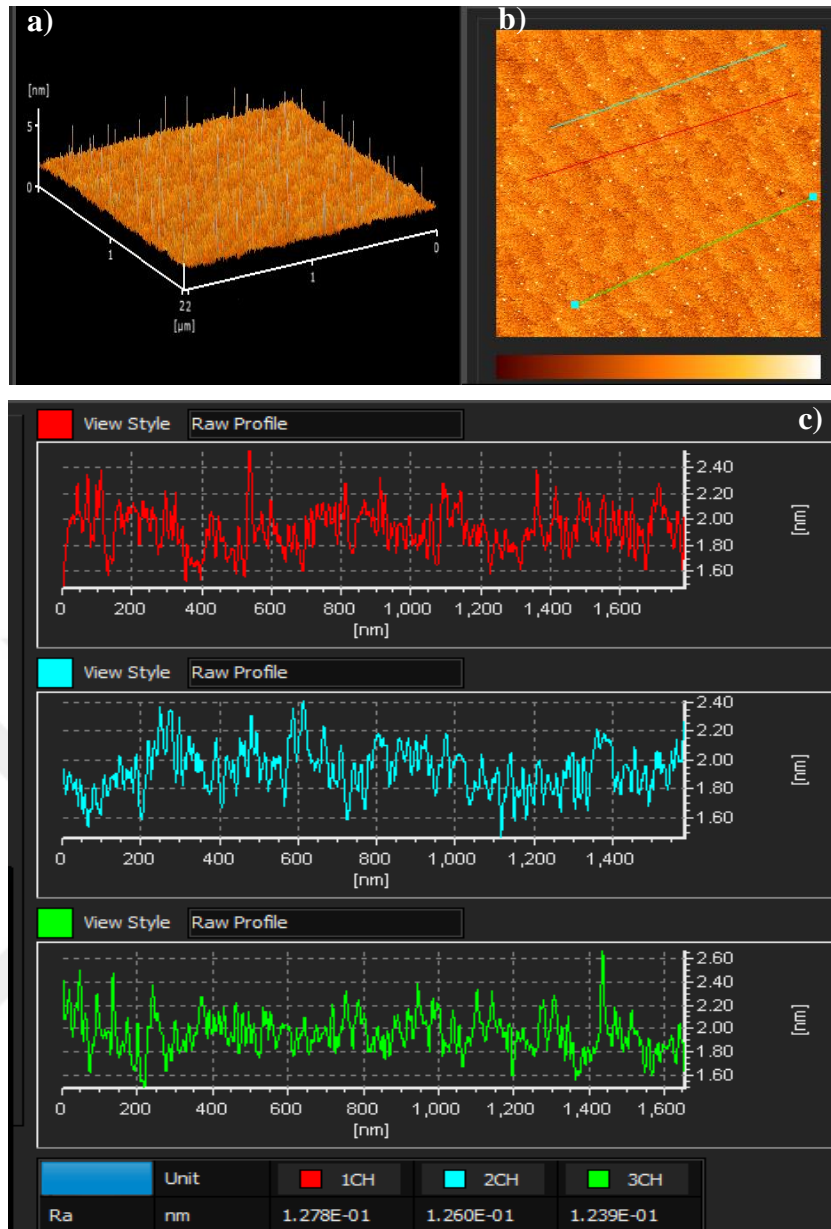
Figure 33. The AFM image of the sample surface deposited at 500 °C

Figure 33.a shows a three-dimensional image in the plane 2 μm × 2 μm and Figure 33.b shows a two-dimensional in the plane 2 μm × 2 μm and Figure 33.c shows linear elevation AFM line height of the sample. Through the reference line, through the red line, the particle height is 2 nm and the roughness is 2.025×10^{-1} nm, the blue line has a particle height of 4.2 nm and the roughness is 3.065×10^{-1} nm, and through the green line it has a particle height of 2 nm and a roughness of 2.079×10^{-1} nm, Figure 33.a shows growth of molecules at a height of 10 nanometers and growth of other molecules at lower heights.

Figure 34. The AFM image of the sample surface deposited at 500 °C and annealed at 30 Torr

Figure 34.a shows a three-dimensional image in the plane 2 μm × 2 μm and Figure 34.b shows a two-dimensional in the plane 2 μm × 2 μm and Figure 34.c shows linear elevation AFM line height of the sample. Through the reference line, through the red line, the particle height is 3.50 nm and the roughness is 3.008×10^{-1} nm, the blue line has a particle height of 1.80 nm and the roughness is 1.321×10^{-1} nm, and through the green line it has a particle height of 2.50 nm and a roughness of 1.556×10^{-1} nm. Figure 34.a shows high roughness and large growth of many nanoparticles with a height of about 4 nanometers, and the image shows high roughness in the area indicated by the red line in image (b).

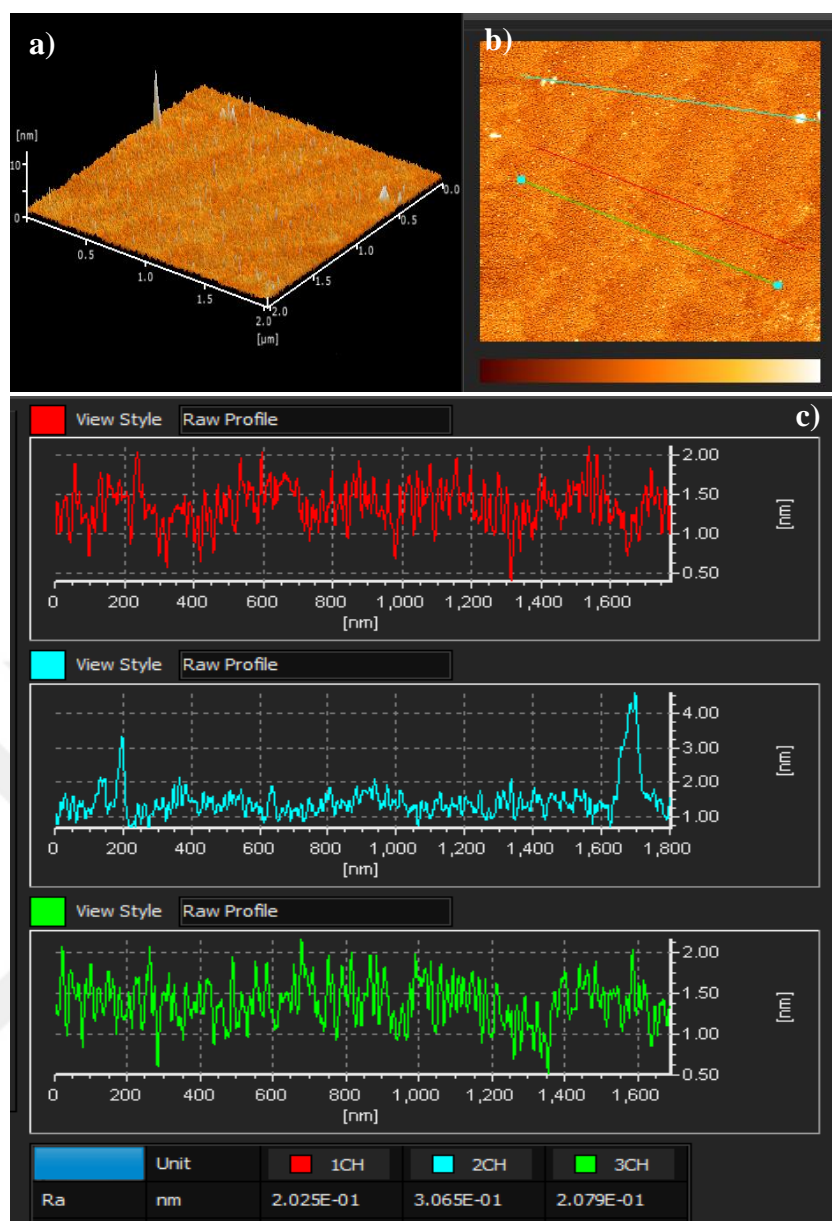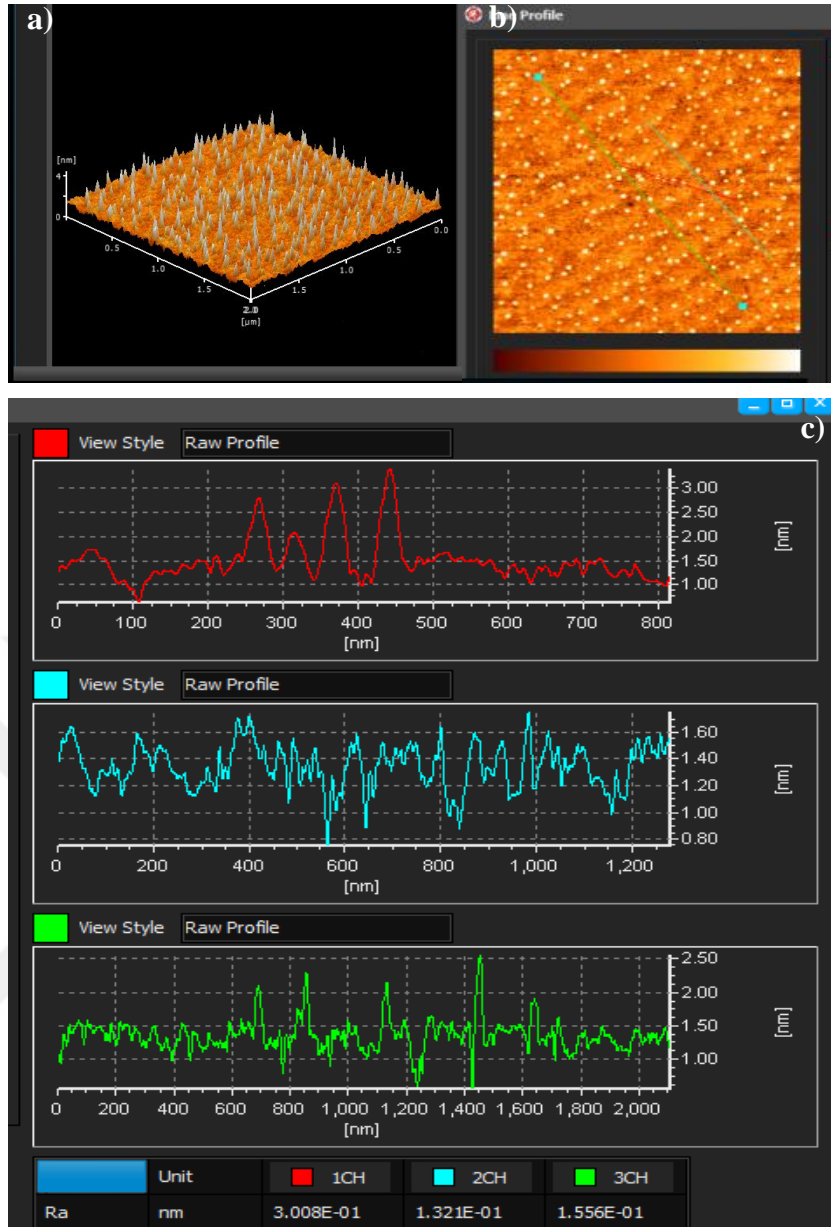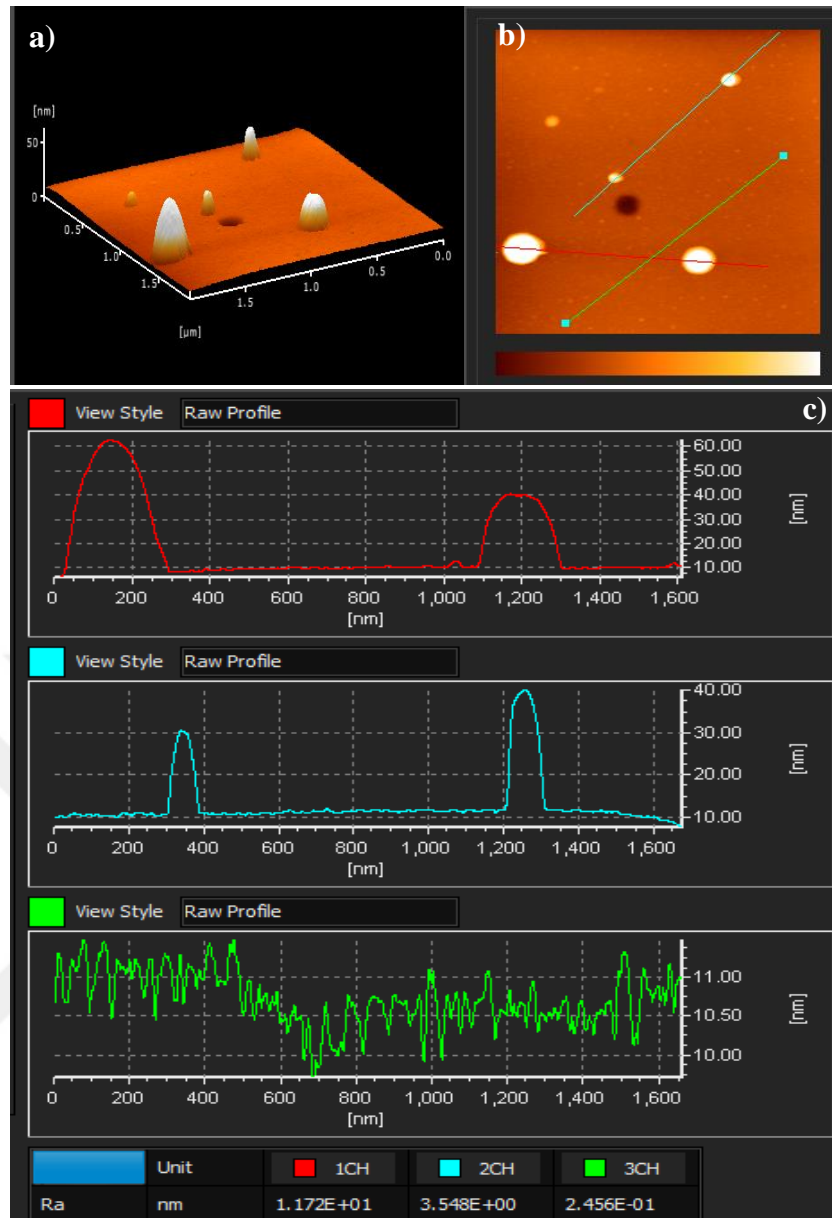**Figure 35.** The AFM image of the sample surface deposited at 600 °C.

Figure 35.a shows a three-dimensional image in the plane 2 μm × 2 μm and Figure 35.b shows a two-dimensional in the plane 2 μm × 2 μm and Figure 35.c shows linear elevation AFM line height of the sample. Through the reference line, through the red line, the particle height is 60 nm and the roughness is $1.172×10^{-1}$ nm, the blue line has a particle height of 40 nm and the roughness is 3.548 nm, and through the green line it has a particle height of 11.70 nm and a roughness of $2.456×10^{-1}$ nm, Figure 35.a shows peak-like growth with a height of 50 nm, high roughness values compared to all previous temperatures.

Comparison of the AFM results revealed that all thin films have very low roughness values. The sample with the lowest roughness value is the thin film prepared at 200 °C. Particles with heights reaching up to 60 nm were detected at temperatures above 500 °C.

It can be observed that increasing the temperature contributed to stimulating the growth of more films and increasing the roughness, this may be due to thermal stress, but it cannot be determined because the increase in temperature during the deposition process may lead to either an increase or a decrease in the surface roughness (Broekmaat et al., 2008). In a study conducted to analyze the surfaces of TiO_2 thin films by Atomic Force Microscopy (AFM), samples were grown at 200, 300, and 400 °C on a silicon substrate by direct current (DC) planar magnetron sputtering system in an O_2/Ar atmosphere. Annealing at higher temperatures generally leads to increased surface roughness and grain growth, with the most significant changes occurring at 400 °C due to more pronounced grain growth at this temperature (Ţălu et al., 2020).The appearance of gaps in the 3D image at 25 °C may be due to defects in the deposition process or non-uniform growth leading to a gap or discontinuity in the film structure. One of the most important reasons for the appearance of gaps is thermal stress during annealing after deposition, as the difference in thermal expansion coefficients between the film and the substrate can lead to stress and the formation of a gap. The reason that can be preferred in this study is the formation of grain boundaries because gaps appeared at 25°C, which means at the temperature at which thin films begin to form and grain growth and their merging in an irregular manner leaves gaps and voids within the film (Jena et al., 2015; Loi et al., 2002; Voigtländer, 2019).

Uneven grain growth can cause grain boundaries to converge and form peak-like structures. Thermal stress can induce surface instabilities that manifest as peaks. The most compelling reason in this study may be due to enhanced surface diffusion. If the deposition temperature is high enough to promote atomic movement, atoms can migrate and aggregate to specific locations and form peaks (Nikam et al., 2020). This is what was observed in peak growth at 600 °C Peak-like structures can be used in optoelectronic devices such as solar cells and photodetectors to enhance light absorption. The peaks can act as effective light traps, improving the device efficiency. Peak-like features on metal thin films can enhance the electromagnetic field at the surface, which is of great importance for Raman spectroscopy (Saritha et al., 2016). Well-controlled temperature promotes regular molecular growth. High temperatures can facilitate the diffusion of atoms, leading to specific crystal structures and regular molecular growth. Regular atomic crystal structures are essential for photovoltaic devices such as LEDs. These materials with regular atomic growth exhibit unique electronic and optical properties due to fewer defects. Films with regular atomic growth tend to have higher mechanical strength and toughness as the uniform structure reduces the possibility of stress concentrations. (Wu et al., 2019)). Looking at the atomic force microscopy results in

this study, regular molecular growth is observed at temperatures of 100 °C, 300 °C, 400 °C, and 500 °C at an annealing pressure of 30 Torr.

Scanning Electron Deposition System Results

SEM images were taken of each film obtained, and the surface morphology of the thin films was determined. The magnifications of the SEM images of the thin films obtained were 10,000x, 20,000x, 50,000x, and 100,000x, respectively (Figure 36-44).
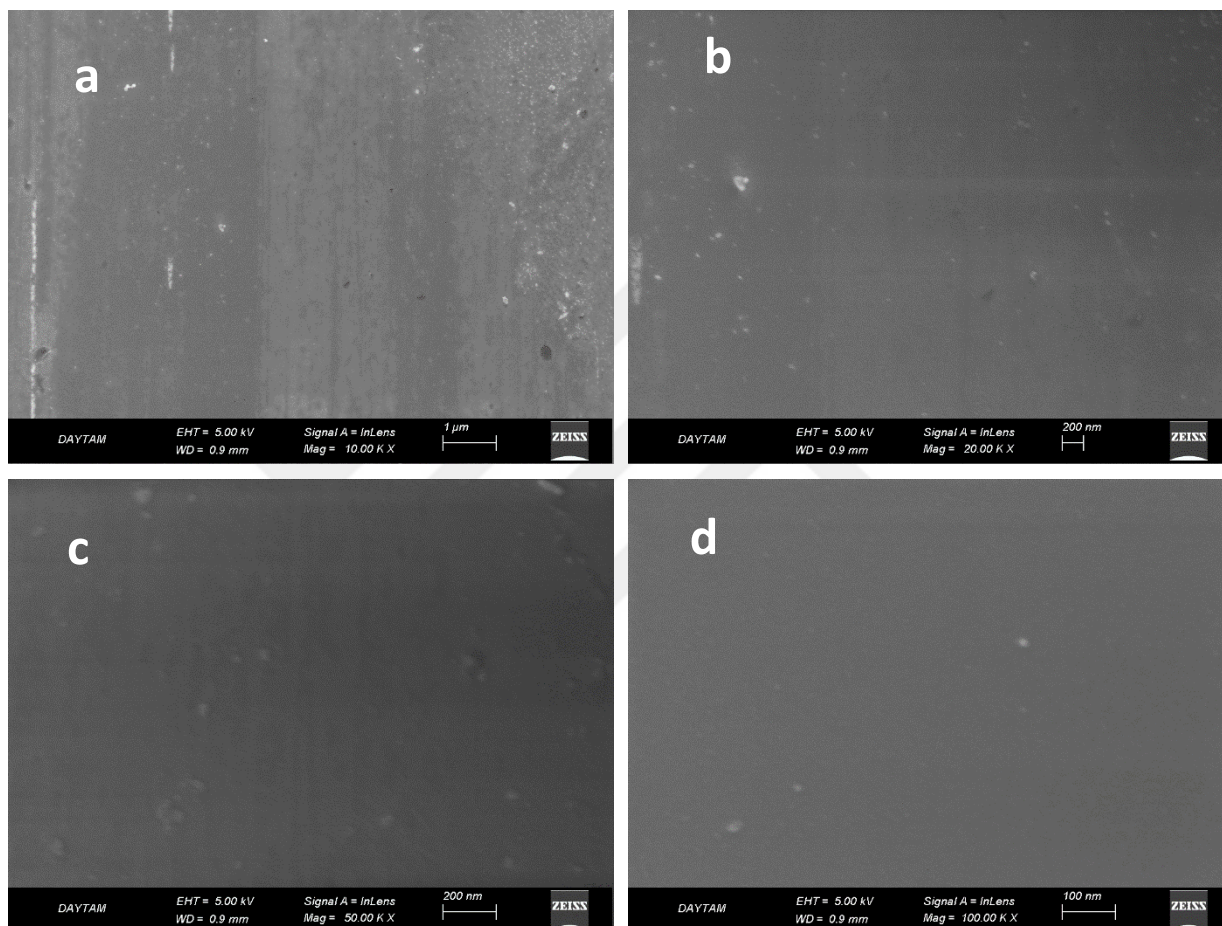
Figure 36. SEM images of the sample surface deposited at 25 °C. a) 10,000x magnification, b) 20,000x magnification, c) 50,000x magnification, d) 100,000x magnification

The Figure 36 shows that the surface not smooth and the surface appears to have a precipitate layer with a simple smooth texture and the growth of small, ill-defined grains due to limited atomic movement at room temperature.
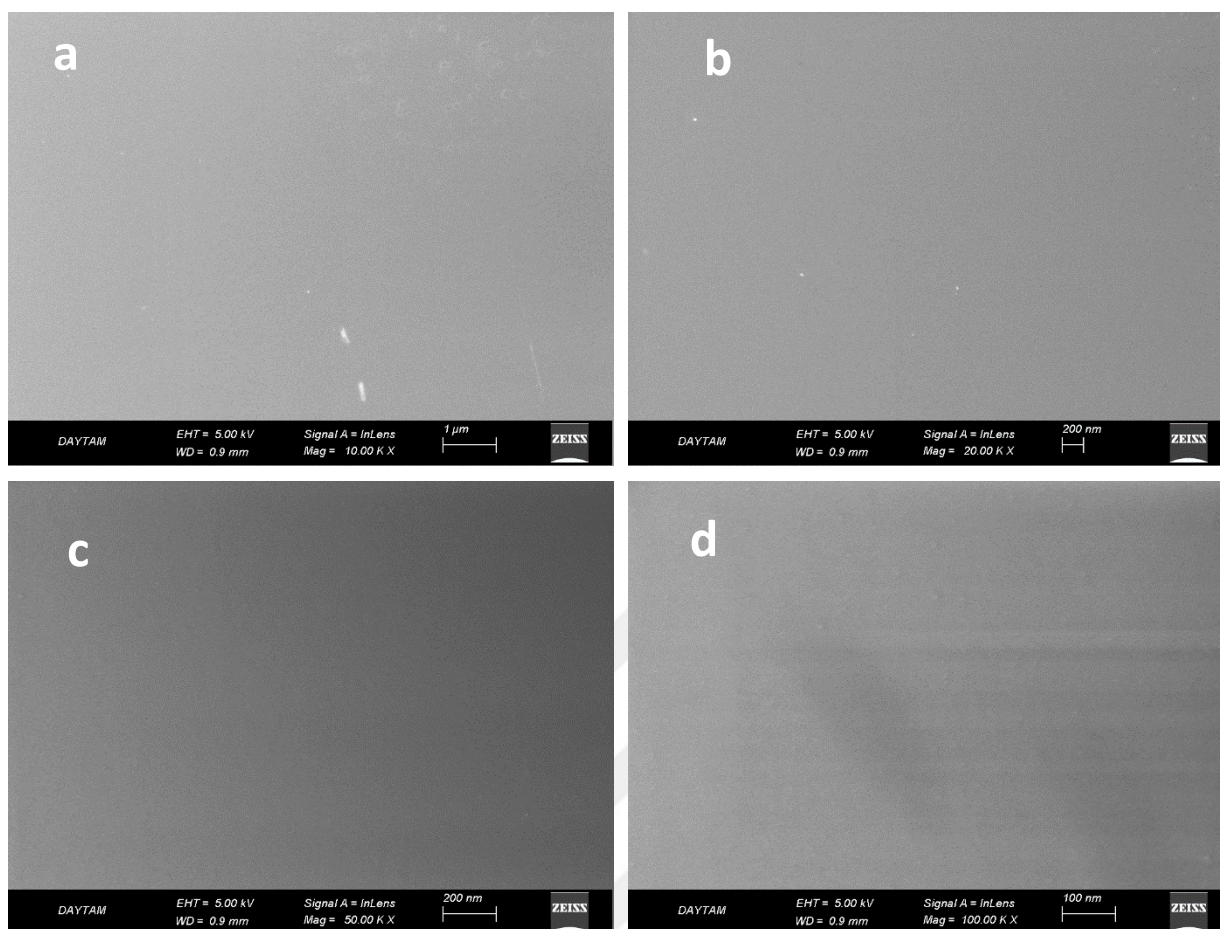
Figure 37. SEM images of the sample surface deposited at 100 °C. a) 10,000x magnification, b) 20,000x magnification, c) 50,000x magnification, d) 100,000x magnification

The Figure 37 shows that the surface very smooth and some small grains grow on the surface.

Figure 38. SEM images of the sample surface deposited at 200 °C. a) 10,000x magnification, b) 20,000x magnification, c) 50,000x magnification, d) 100,000x magnification.

The Figure 38 shows that the surface is very smooth
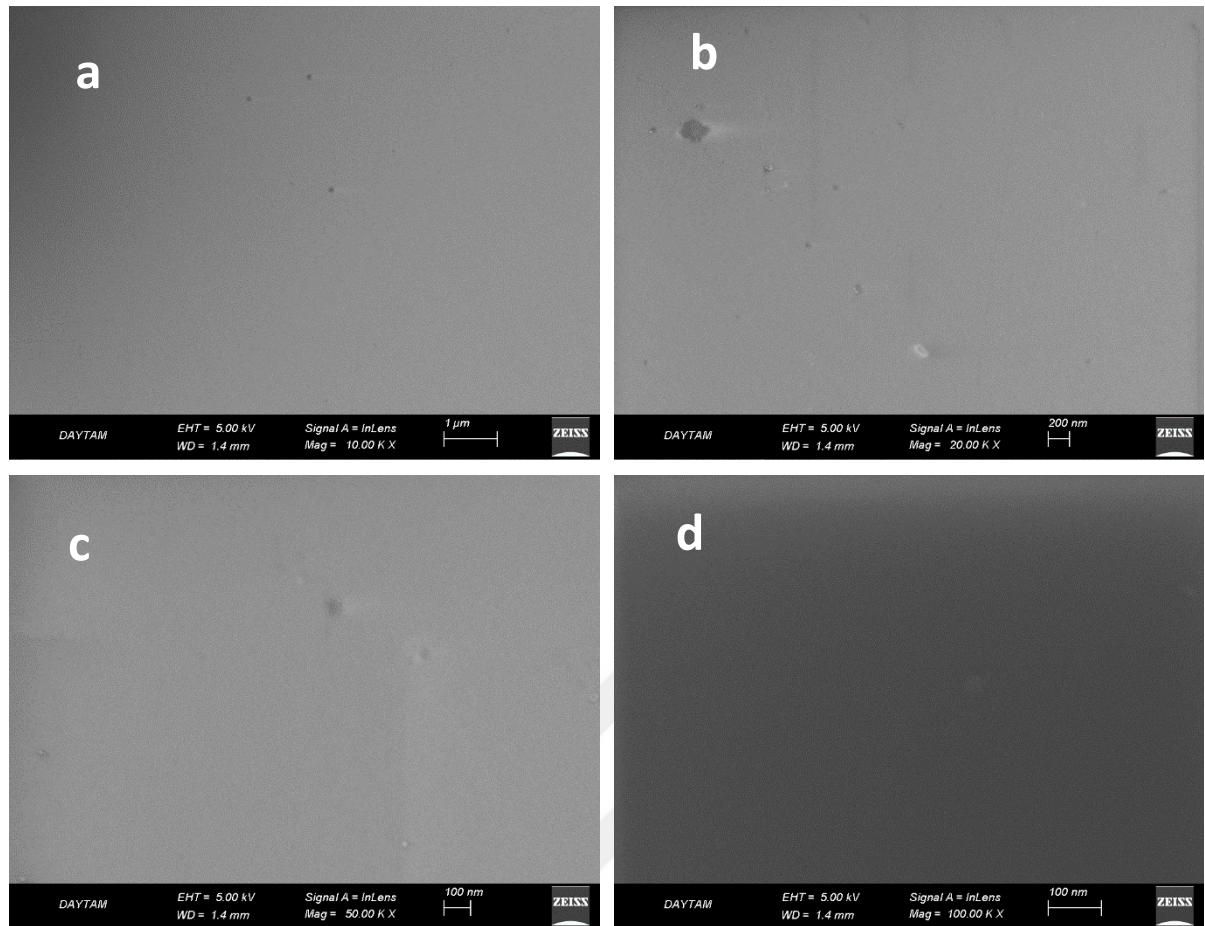
Figure 39. SEM images of the sample surface deposited perpendicular at 200 °C. a) 10,000x magnification, b) 20,000x magnification, c) 50,000x magnification, d) 100,000x magnification

Figure 39 shows that the surface is smooth but has dents, and some small grains grew on the surface. Placing the substrate perpendicular dramatically reduced surface roughness.
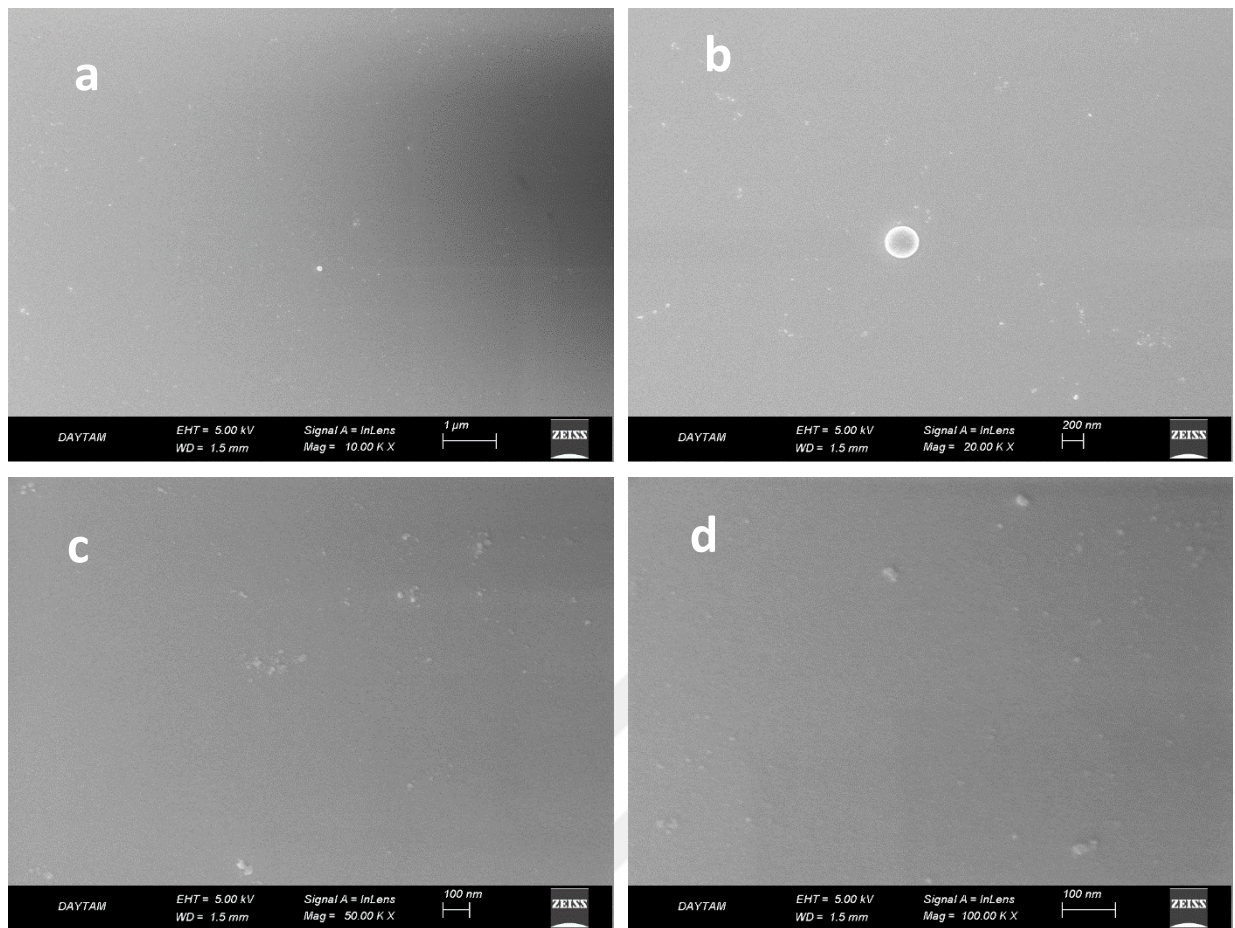
Figure 40. SEM images of the sample surface deposited at 300 °C. a) 10,000x magnification, b) 20,000x magnification, c) 50,000x magnification, d) 100,000x magnification

Figure 40 shows that the surface has a droplet with 200 nm diameter and surface is smooth but has lots of small particles. Rise in the temperature resulted rough surface.
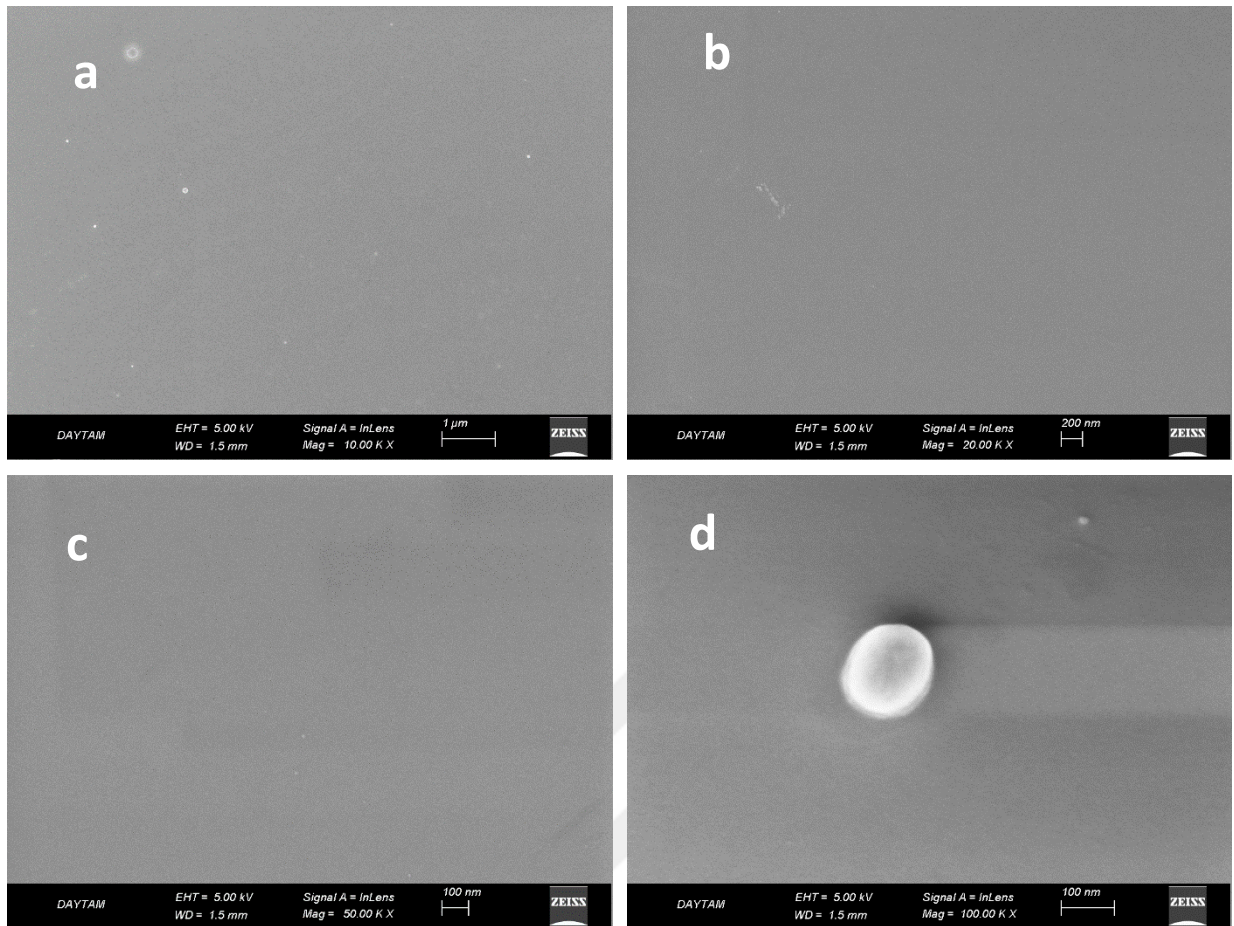
Figure 41. SEM images of the sample surface deposited at 400 °C. a) 10,000x magnification, b) 20,000x magnification, c) 50,000x magnification, d) 100,000x magnification

Figure 41 shows that the surface has a droplet with a 100 nm diameter, and most of the surface area is flat, Image (d) shows a large droplet particle.
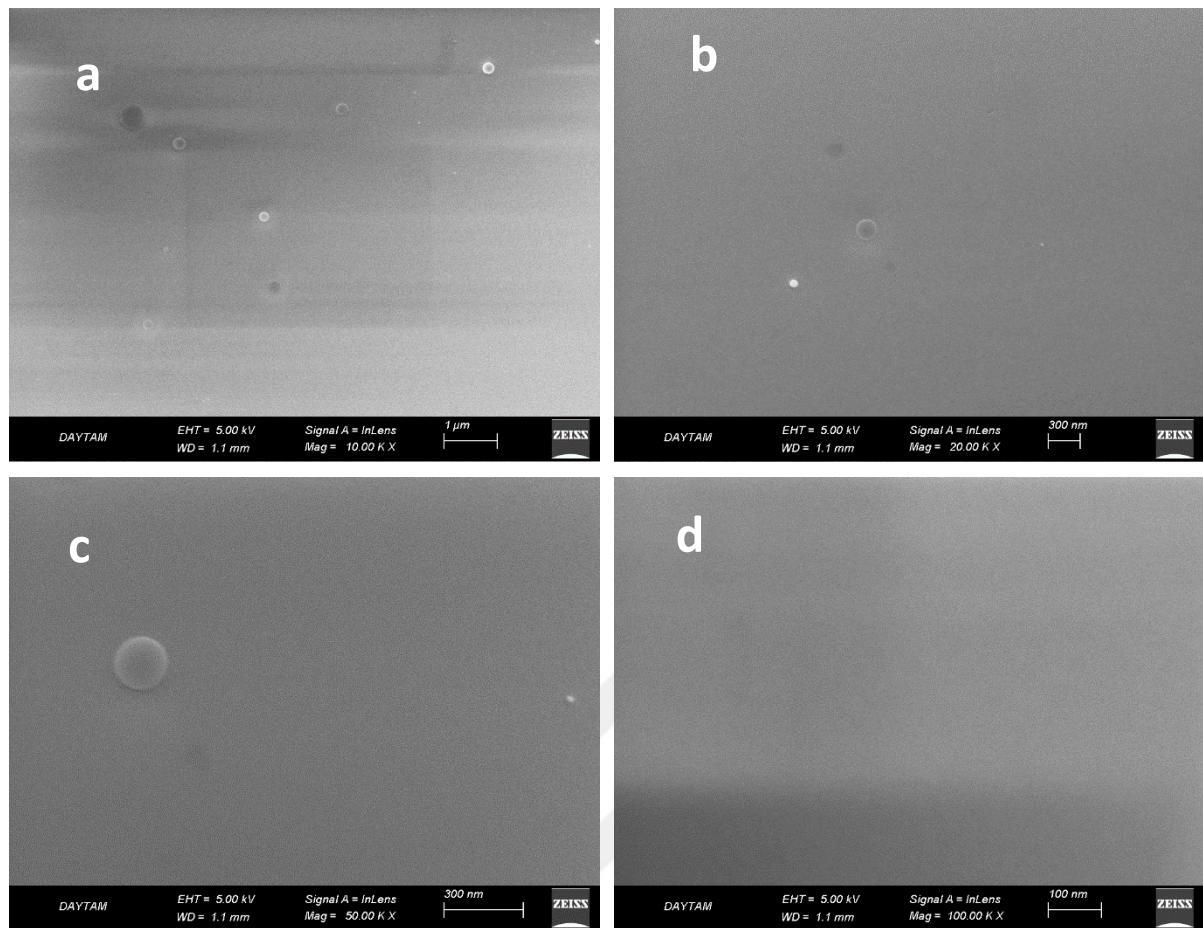
Figure 42. SEM images of the sample surface deposited at 500 °C. a) 10,000x magnification, b) 20,000x magnification, c) 50,000x magnification, d) 100,000x magnification

Figure 42 shows that the surface has a few droplets but is generally smooth.
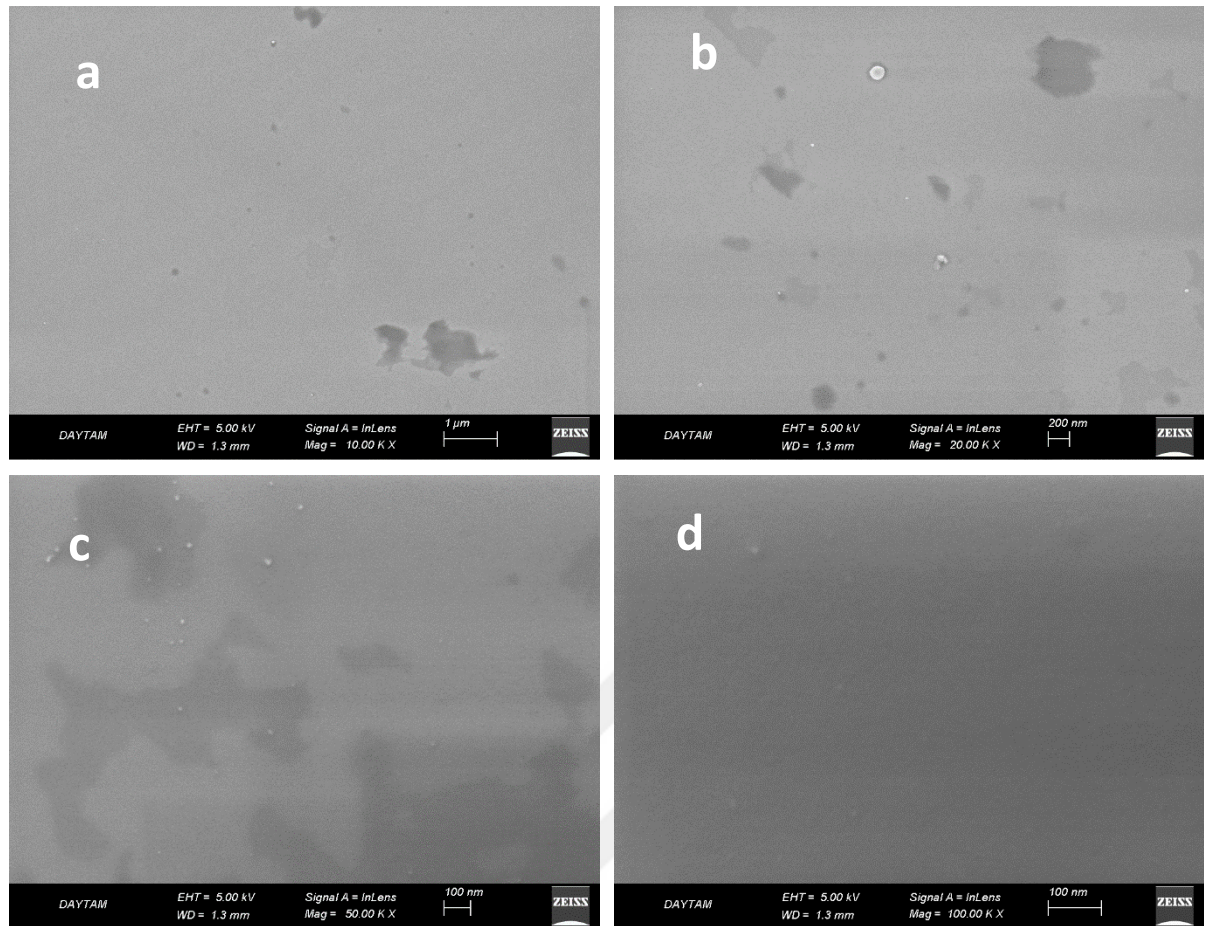
Figure 43. SEM images of the sample surface deposited at 500 °C and annealed at 30 Torr. a) 10,000x magnification, b) 20,000x magnification, c) 50,000x magnification, d) 100,000x magnification

Figure 43 shows that the surface has different domains and is rougher compared to the standard annealing temperature.
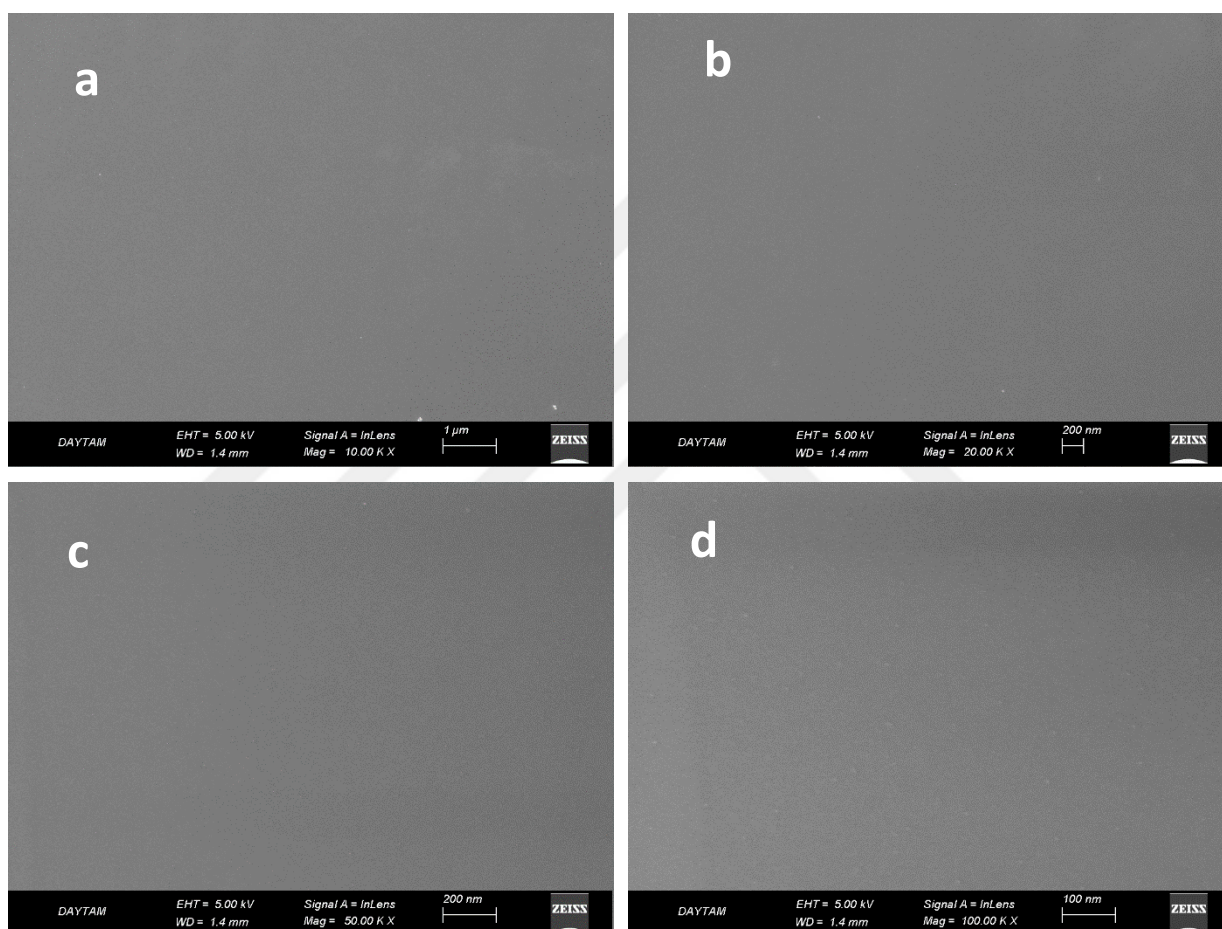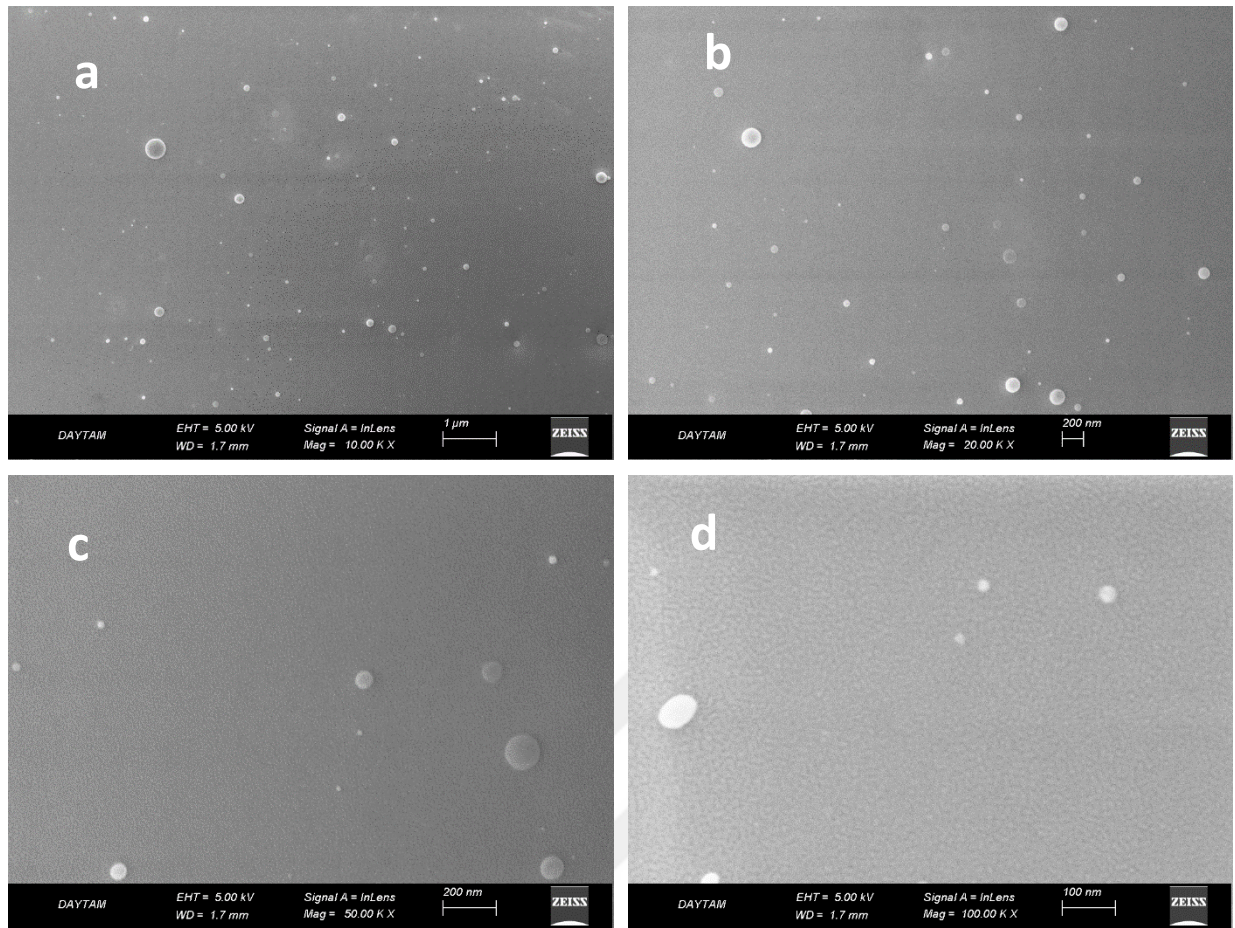
Figure 44. SEM images of the sample surface deposited at 600 °C. a) 10,000x magnification, b) 20,000x magnification, c) 50,000x magnification, d) 100,000x magnification.

Figure 44 shows that all the surfaces have many droplets with sizes varying from 1 μm to 200 nm and 100 nm. The maximum zoom reveals a compact network growth of nanoparticles and the surface is fused and is not as smooth as previous samples.

Based on the scanning electron microscope results, most of the thin films have smooth surfaces at temperatures of 100 °C, 200 °C, perpendicular 200 °C, 300 °C and 400 °C. Smooth surface thin films are widely used in various industries and research fields. Their applications include optical coatings, mirrors, semiconductor devices, transistors, and photovoltaics and Smooth thin films are considered resistant to corrosion and scratches (Pascu et al., 2022). The results show that at a temperature of 500 °C and an annealing pressure of 30 Torr, the film surface contains domains due to the change in annealing pressure. It was concluded that the sample annealed at 200 °C has the smoothest surface compared to all other samples. The results show that at temperatures of 500 °C and above, droplets appear on the surface, making deposition above 500 °C not recommended. The surface of the film at a temperature of 600 °C contains a rough surface with large crystalline grains resembling a network at a magnification of 100.000 times.

In a study conducted using PLD for ZnO deposition (Verardi et al., 1999), where a scanning electron microscope was used for surface analysis, the results indicate slightly rough nanoscale surfaces for the thin films (smooth). By comparing these findings with those obtained in this study, ZnO was studied by PLD in an atmosphere of high purity oxygen. This same step was carried out in this study to deposit cerium oxide. The present study have proven that high-purity oxygen contributes to obtaining smoother and more uniform film surfaces by preventing unwanted chemical reactions or impurities that can disrupt film growth, as proven by many studies (Banerjee et al., 2020; Sekkat et al., 2021)

Placing the sample perpendicular at 200 °C is not preferable due to dents and small grains. Deposition at high temperatures results in droplets on the sample surface, so deposition at temperatures higher than 500 °C is not recommended. Annealing at 15 Torr is sufficient, and increasing the annealing pressure leads to the formation of domains on the surface. Since controlled cooling was done at 10 °C/min, no cracks have formed on any of the sample surfaces due to differences in the thermal expansion coefficients of the substrate and the thin film.

X-ray photoelectron spectroscopy (XPS) results

X-ray photoelectron spectroscopy (XPS) is a surface-sensitive quantitative spectroscopic technique that measures the very topmost 200 atoms, 0.01 um, 10 nm of any surface. In order to determine the chemical composition of the prepared thin films, an XPS scan was conducted on the sample prepared at 300 °C with a Specs-Flex XPS. The result show that the surface of the thin film contains only two elements: cerium and oxygen, as shown in Figure 45 below. Due to the prolonged waiting time for XPS analysis, the sample was oxidized during this period, and the cerium oxide phase could not be determined.

Ce 3p3/2
Ce 3p

Name	Pos.	FWHM	Area	At%
Ce 3d5/2	881.00	5.575	18742.3	14.826
O 1s	528.00	3.904	10343.5	85.174
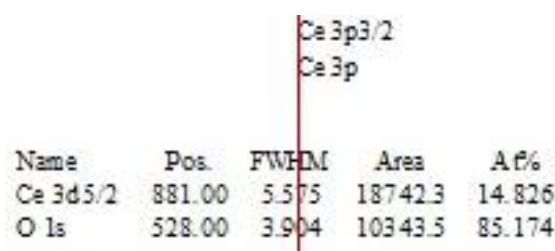
Figure 45. XPS data of thin films of cerium oxide.

The X-ray Photoelectron Spectroscopy (XPS) survey of the thin film revealed the presence of only two elements: cerium (Ce) and oxygen (O). The absence of other elemental signals in the spectrum confirms the film's high purity and suggests successful deposition of the Ce-O compound. The relative intensity of the Ce and O peaks can provide insights into the stoichiometry of the film, which is critical for understanding its structural and functional

properties. However, the long wait for analysis resulted in oxidation of the samples and it was not possible to identify the cerium-oxide phase by XPS method, but XRD results clearly show Ce_2O_3 phase. This result highlights the effectiveness of the deposition process in achieving a controlled and homogenous composition.

CONCLUSION AND RECOMMENDATIONS

PED technology is widely used for the deposition and preparation of thin and thick films. The stoichiometry of the target material is maintained during transfer to the substrate. It is a fast crystal growth method, allows for the preparation of superlattices thanks to the use of multiple targets, and enables samples to be annealed without removing them from the vacuum chamber. This makes the method a very effective physical deposition technique.

In this study, Cerium Oxide thin film growth was performed using a PED system. For this purpose, LAO with suitable crystal lattice and thermal expansion coefficient was chosen as a substrate and high quality; Cerium Oxide thin films were obtained with one high intensity GIXRD peak (Figure 17) referring to Ce_2O_3 for growth temperatures from room temperature to 600 °Deep GIXRD analysis of thin films for very low intensity peaks revealed that the thin films comprise three types of cerium oxide: CeO_2, Ce_2O_3, and Ce_7O_{12}.

The crystalline properties, surface morphology, and homogeneity of the prepared samples were evaluated by Grazing Incidence X-ray diffraction (GIXRD), scanning electron microscopy (SEM), atomic force microscopy (AFM) and X-Ray photoelectric spectroscopy (XPS).

The XPS results indicate that the deposited thin films are composed solely of cerium and oxygen atoms. The GIXRD analysis showed that the samples grown at temperatures of 300 °C, 400 °C, and 500 °C exhibited the highest level of crystallinity. However, after taking into account the peak associated with Ce_7O_{12} at 55°, the most optimal sample was selected as the one that was cultivated at 300 °C.

The graph between the roughness value obtained from the results of the AFM device and the temperatures, as shown in Figure 46, where deposition occurred in each experiment, shows the presence of continued growth of smooth surfaces at all temperatures and the growth of very rough surfaces at 600 °C.

Upon comparing the AFM results, it was found that all thin films exhibit extremely low roughness values. The thin film prepared at 200 °C exhibits the minimum roughness value among the samples. Nanoparticles with heights of up to 60 nm were observed at temperatures exceeding 500 °C.

Roughness and temperature
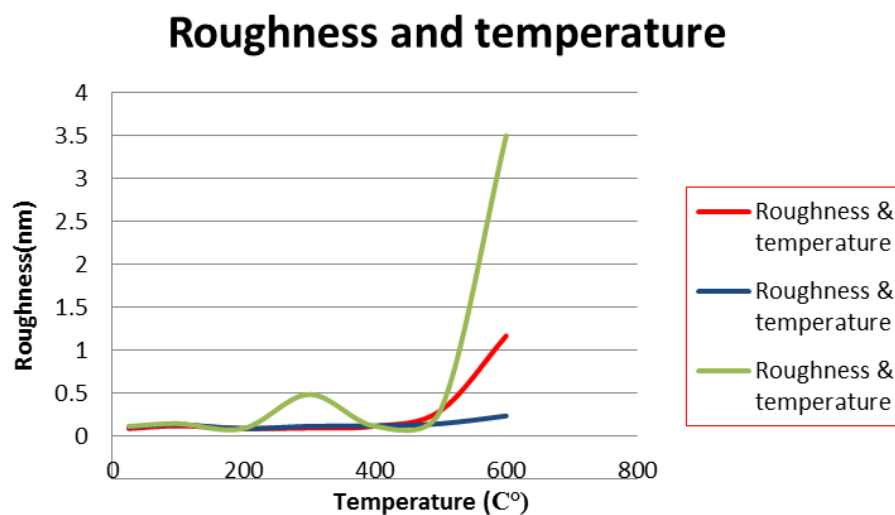
Figure 46. Roughness values for cerium oxide thin films as a function of deposition temperature.

Based on the SEM results, all thin films have smooth surfaces at temperatures of 100 °C, 200 °C, 200 °C perpendicular, 300 °C, and 400 °C. The SEM images of thin film of cerium oxide at an annealing pressure of 30 Torr and a temperature of 500 °C show a surface containing domain areas comparing with all other surface results due to the change in annealing pressure. The sample with the most polished surface is the one grown at 200 °C. It is not advisable to position the sample at a 90-degree angle at this temperature due to the risk of dents and small grains. Deposition at elevated temperatures leads to the formation of small liquid droplets on the sample surface, so deposition above 500 °C is not recommended. The thin film prepared at 600 °C has a rough surface with large crystalline grains that resemble compact tissue, due to the high temperature. Annealing at a pressure of 15 Torr is sufficient; increasing the annealing pressure creates domains on the surface.

Cerium oxide, especially its form Ce_2O_3, plays an important role in applications that require smooth surfaces due to its unique physical and chemical properties, including the use of cerium as a polishing agent in the glass industry and the creation of exceptionally smooth surfaces in optical mirrors and lenses. The smooth surface of cerium oxide is useful in various chemical catalytic processes, as it enhances selective reaction rates by providing a stable and active site. Research in recent years indicates the use of cerium oxide in the production of solid oxide fuel cell components, where a smooth surface is critical for effective ion doping and fuel oxidation. (N. Chakrabarty, 2021)

When comparing the results of this study with the results of deposition of cerium oxide by PLD, the surfaces deposited by PED are smoother compared to the results of PLD (Yurtcan, 2021), which showed a network-like surface formation. The superiority in the

results in both studies is attributed to the specific properties targeted by a particular application. For example, smooth nano-surfaces are usually characterized by less friction due to the absence of roughness, which is beneficial in mechanical resistance and light scattering. As for nano-surfaces that have a network shape, they help increase the surface area, which enhances interaction with other materials. This property plays a major role in applications such as catalysis and energy storage. These networked nano-surfaces can also be used to enhance adhesion and strong bonding in composite materials such as paints. They can also manipulate and disperse light, which is useful in photovoltaic cells and sensors. In conclusion, determining the choice between surfaces depends on the specific requirements of the intended application, as each of them provides properties that suit different functional needs. (Li et al., 2024).

In a study on coating thin films of CeO_2 doped with Er using PED, X-ray diffraction measurements indicated that all films are polycrystalline with an FCC (Face-Centered Cubic) structure, and that Er doping affects the X-ray diffraction patterns of cerium oxide films (Tatar et al., 2013). While in this study all thin films have one significant very high intensity peak corresponding to hexagonal Ce_2O_3. CeO_2 (FCC) is more stable, versatile, and widely used, making it the preferred choice for many applications (Kusmierek, 2020). Especially, Ce_2O_3 (hexagonal) has unique properties that can be useful in redox applications (Upolovnikova et al., 2024).

As a result, cerium oxide thin films can be obtained at various temperatures using the PED method on LAO substrates. To achieve a flat surface, samples should be prepared at temperatures between 100 °C and 400 °C, particularly at 200 °C. For the best Ce_2O_3 crystallinity, thin films should be prepared at 300 °C for PED method. In order to obtain thin films with the desired properties, variables such as energy, frequency, coating pressure, etc., can be optimized further.

REFERENCES

Abegunde, O. O., Akinlabi, E. T., Oladijo, O. P., Akinlabi, S., & Ude, A. U. (2019). Overview of thin film deposition techniques. *AIMS Materials Science*, *6*(2), 174–199.

Alves, N., Ferraz, W. B., & Faria, L. O. (2014). Synthesis and investigation of the luminescent properties of carbon doped lanthanum aluminate (LaAlO3) for application in radiation dosimetry. *Radiation Measurements*, *71*, 90–94.

Andrade, J. D. (1985). X-ray photoelectron spectroscopy (XPS). *Surface and Interfacial Aspects of Biomedical Polymers: Volume 1 Surface Chemistry and Physics*, 105–195.

Andrle, A., Hönicke, P., Gwalt, G., Schneider, P.-I., Kayser, Y., Siewert, F., & Soltwisch, V. (2021). Shape-and element-sensitive reconstruction of periodic nanostructures with grazing incidence x-ray fluorescence analysis and machine learning. *Nanomaterials*, *11*(7), 1647.

Arachi, Y., Sakai, H., Yamamoto, O., Takeda, Y., & Imanishai, N. (1999). Electrical conductivity of the ZrO2–Ln2O3 (Ln= lanthanides) system. *Solid State Ionics*, *121*(1–4), 133–139.

Arisi, E., Bergenti, I., Cavallini, M., Murgia, M., Riminucci, A., Ruani, G., & Dediu, V. (2007). Room temperature deposition of magnetite thin films on organic substrate. *Journal of Magnetism and Magnetic Materials*, *316*(2), 410–412.

Asha, A. B., & Narain, R. (2020). Nanomaterials properties. In *Polymer science and nanotechnology* (pp. 343–359). Elsevier.

Aziz, M., & Ismail, A. F. (2017). X-ray photoelectron spectroscopy (XPS). In *Membrane Characterization* (pp. 81–93). Elsevier.

Banerjee, S., Adhikari, E., Sapkota, P., Sebastian, A., & Ptasinska, S. (2020). Atmospheric pressure plasma deposition of TiO2: A review. *Materials*, *13*(13), 2931.

Bellucci, D., Bianchi, M., Graziani, G., Gambardella, A., Berni, M., Russo, A., & Cannillo, V. (2017). Pulsed Electron Deposition of nanostructured bioactive glass coatings for biomedical applications. *Ceramics International*, *43*(17), 15862–15867.

Bleu, Y., Bourquard, F., Tite, T., Loir, A.-S., Maddi, C., Donnet, C., & Garrelie, F. (2018). Review of graphene growth from a solid carbon source by pulsed laser deposition (PLD). *Frontiers in Chemistry*, *6*, 572.

Broekmaat, J., Brinkman, A., Blank, D. H. A., & Rijnders, G. (2008). High temperature surface imaging using atomic force microscopy. *Applied Physics Letters*, *92*(4).

Creighton, J., & Ho, P. (2001). Introduction to Chemical Vapor Deposition (CVD). *ASM International*.

Darquenne, C. (2020). Deposition mechanisms. *Journal of Aerosol Medicine and Pulmonary Drug Delivery*, *33*(4), 181–185.

Depla, D., Mahieu, S., & Greene, J. E. (2010). Sputter deposition processes. In *Handbook of*

deposition technologies for films and coatings (pp. 253–296). Elsevier.

Devreese, J. T. (2007). Importance of nanosensors: Feynman's vision and the birth of nanotechnology. *MRS Bulletin*, *32*(9), 718–725.

Dhall, A., & Self, W. (2018). Cerium oxide nanoparticles: a brief review of their synthesis methods and biomedical applications. *Antioxidants*, *7*(8), 97.

Dowding, J. M., Song, W., Bossy, K., Karakoti, A., Kumar, A., Kim, A., Bossy, B., Seal, S., Ellisman, M. H., & Perkins, G. (2014). Cerium oxide nanoparticles protect against Aβ-induced mitochondrial fragmentation and neuronal cell death. *Cell Death & Differentiation*, *21*(10), 1622–1632.

Dubes, A., Parrot-Lopez, H., Abdelwahed, W., Degobert, G., Fessi, H., Shahgaldian, P., & Coleman, A. W. (2003). Scanning electron microscopy and atomic force microscopy imaging of solid lipid nanoparticles derived from amphiphilic cyclodextrins. *European Journal of Pharmaceutics and Biopharmaceutics*, *55*(3), 279–282.

Dutta, P. (2000). Grazing incidence X-ray diffraction. *Current Science*, 1478–1483.

Eaton, P., & West, P. (2010). *Atomic force microscopy*. Oxford university press.

Elmer, W., & White, J. C. (2018). The future of nanotechnology in plant pathology. *Annual Review of Phytopathology*, *56*(1), 111–133.

Feng, X., Chen, R., Nan, Z., Lv, X., Meng, R., Cao, J., & Tang, Y. (2019). Perfection of perovskite grain boundary passivation by Eu-porphyrin complex for overall-stable perovskite solar cells. *Advanced Science*, *6*(5), 1802040.

Franzini, M., Leoni, L., & Lezzerini, M. (2000). A procedure for determining the chemical composition of binder and aggregate in ancient mortars: its application to mortars from some medieval buildings in Pisa. *Journal of Cultural Heritage*, *1*(4), 365–373.

Fu, Y., Li, J., & Li, J. (2019). Metal/semiconductor nanocomposites for photocatalysis: fundamentals, structures, applications and properties. *Nanomaterials*, *9*(3), 359.

Fujioka, H. (2015). Pulsed laser deposition (PLD). In *Handbook of Crystal Growth* (pp. 365–397). Elsevier.

Gao, Y., Chen, K., Ma, J., & Gao, F. (2014). Cerium oxide nanoparticles in cancer. *OncoTargets and Therapy*, 835–840.

Gupta, A., Das, S., Neal, C. J., & Seal, S. (2016). Controlling the surface chemistry of cerium oxide nanoparticles for biological applications. *Journal of Materials Chemistry B*, *4*(19), 3195–3202.

Han, B., Tomer, V., Nguyen, T. A., Farmani, A., & Singh, P. K. (2020). *Nanosensors for smart cities*. Elsevier.

Higashisaka, K., Yoshioka, Y., & Tsutsumi, Y. (2015). Applications and safety of nanomaterials used in the food industry. *Food Safety*, *3*(2), 39–47.

Hoshino, T., Aoki, S., Itoh, M., Itoh, H., Inoue, T., & Matsuyama, S. (2024). Examination of measurement by hard X-ray grazing incidence diffraction patterns of isolated lattices for 3D 1-nm resolution. *Optical Engineering*, *63*(11), 111804.

Hulla, J. E., Sahu, S. C., & Hayes, A. W. (2015). Nanotechnology: History and future. *Human*

    & Experimental Toxicology, *34*(12), 1318–1321.

Inbaraj, B. S., & Chen, B.-H. (2020). An overview on recent in vivo biological application of cerium oxide nanoparticles. *Asian Journal of Pharmaceutical Sciences*, *15*(5), 558–575.

Ivanov, V. K., Shcherbakov, A. B., & Usatenko, A. V. (2009). Structure-sensitive properties and biomedical applications of nanodispersed cerium dioxide. *Russian Chemical Reviews*, *78*(9), 855.

Jena, S., Tokas, R., Thakur, S., & Sahoo, N. K. (2015). Characterization of optical thin films by spectrophotometry and atomic force microscopy. *SMC Bulletin*, *6*(1), 1–9.

Kaiser, N. (2002). Review of the fundamentals of thin-film growth. *Applied Optics*, *41*(16), 3053–3060.

Kaur, R., Sharma, S. K., & Tripathy, S. K. (2019). Advantages and limitations of environmental nanosensors. In *Advances in nanosensors for biological and environmental analysis* (pp. 119–132). Elsevier.

Kusmierek, E. (2020). A CeO2 semiconductor as a photocatalytic and photoelectrocatalytic material for the remediation of pollutants in industrial wastewater: a review. *Catalysts*, *10*(12), 1435.

Li, W., Xin, Q., Fan, B., Chen, Q., & Deng, Y. (2024). A Review of Emerging Technologies in Ultra-Smooth Surface Processing for Optical Components. *Micromachines*, *15*(2), 178.

Liguori, A., Gualandi, C., Focarete, M. L., Biscarini, F., & Bianchi, M. (2019). The pulsed electron deposition technique for biomedical applications: A review. *Coatings*, *10*(1), 16.

Loi, S., Sun, G., Franz, V., & Butt, H.-J. (2002). Rupture of molecular thin films observed in atomic force microscopy. II. Experiment. *Physical Review E*, *66*(3), 31602.

Lotz, B., Wittmann, J. C., & Lovinger, A. J. (1996). Structure and morphology of poly (propylenes): a molecular analysis. *Polymer*, *37*(22), 4979–4992.

Mathis, J. E., & Christen, H. M. (2007). Factors that influence particle formation during pulsed electron deposition of YBCO precursors. *Physica C: Superconductivity*, *459*(1–2), 47–51.

Mazzer, M., Rampino, S., Gombia, E., Bronzoni, M., Bissoli, F., Pattini, F., Calicchio, M., Kingma, A., Annoni, F., & Calestani, D. (2016). Progress on low-temperature pulsed electron deposition of CuInGaSe2 solar cells. *Energies*, *9*(3), 207.

Michler, G. H. (2008). *Scanning electron microscopy (SEM)*. Springer.

Mirshojaeian Hosseini, M. J., & Nawrocki, R. A. (2021). A review of the progress of thin-film transistors and their technologies for flexible electronics. *Micromachines*, *12*(6), 655.

Nikam, S. M., Sharma, A., Rahaman, M., Teli, A. M., Mujawar, S. H., Zahn, D. R. T., Patil, P. S., Sahoo, S. C., Salvan, G., & Patil, P. B. (2020). Pulsed laser deposited CoFe 2 O 4 thin films as supercapacitor electrodes. *RSC Advances*, *10*(33), 19353–19359.

Pascu, R. V., Epurescu, G., Boerasu, I., Niculescu, A.-M. B., Manica, D., Trefilov, A. M. I., & Sava, B. A. (2022). Samarium doped cerium oxide thin films deposited by pulsed laser deposition. *Applied Surface Science*, *606*, 154994.

Pinto, H., Mintz, M. H., Melamud, M., & Shaked, H. (1982). Neutron diffraction study of Ce2O3. *Physics Letters A*, *88*(2), 81–83.

Riu, J., Maroto, A., & Rius, F. X. (2006). Nanosensors in environmental analysis. *Talanta*, *69*(2), 288–301.

Saritha, A. C., Shijeesh, M. R., Vikas, L. S., Prabhu, R. R., & Jayaraj, M. K. (2016). Growth and characterization of p-ZnO: Cu thin film and its homojunction application. *Journal of Physics D: Applied Physics*, *49*(29), 295105.

Sato, M., Kawata, A., Morito, S., Sato, Y., & Yamaguchi, I. (2008). Preparation and properties of polymer/zinc oxide nanocomposites using functionalized zinc oxide quantum dots. *European Polymer Journal*, *44*(11), 3430–3438.

Schock, H. W. (1996). Thin film photovoltaics. *Applied Surface Science*, *92*, 606–616.

Sekkat, A., Bellet, D., Chichignoud, G., Kaminski-Cachopo, A., Muñoz-Rojas, D., & Favre, W. (2021). Open-air, low-temperature deposition of phase pure Cu 2 O thin films as efficient hole-transporting layers for silicon heterojunction solar cells. *Journal of Materials Chemistry A*, *9*(29), 15968–15974.

Shahidi, S., Moazzenchi, B., & Ghoranneviss, M. (2015). A review-application of physical vapor deposition (PVD) and related methods in the textile industry. *The European Physical Journal Applied Physics*, *71*(3), 31302.

Stokes, D. (2008). *Principles and practice of variable pressure/environmental scanning electron microscopy (VP-ESEM)*. John Wiley & Sons.

Strikovski, M. D., Kim, J., & Kolagani, S. H. (2010). Plasma energetics in pulsed laser and pulsed electron deposition. *Springer Handbook of Crystal Growth*, 1193–1211.

Ţălu, Ş., Achour, A., Solaymani, S., Nikpasand, K., Dalouji, V., Sari, A., Rezaee, S., & Nezafat, N. B. (2020). Micromorphology analysis of TiO2 thin films by atomic force microscopy images: The influence of postannealing. *Microscopy Research and Technique*, *83*(5), 457–463.

Tatar, B., Gökdemir, F. P., Pehlivan, E., & Urgen, M. (2013). The influence of Er3+ doping on the structural and optical properties of CeO2 thin films grown by PED. *Applied Surface Science*, *285*, 409–416.

Upolovnikova, A. G., Shartdinov, R. R., & Smetannikov, A. N. (2024). Study of the process of cerium restoration by aluminum and calcium carbide from cerium-containing slag. *Rasplavy*, *1*, 26–35.

Vaynzof, Y. (2020). The future of perovskite photovoltaics—thermal evaporation or solution processing? *Advanced Energy Materials*, *10*(48), 2003073.

Verardi, P., Nastase, N., Gherasim, C., Ghica, C., Dinescu, M., Dinu, R., & Flueraru, C. (1999). Scanning force microscopy and electron microscopy studies of pulsed laser deposited ZnO thin films: application to the bulk acoustic waves (BAW) devices. *Journal of Crystal Growth*, *197*(3), 523–528.

Voigtländer, B. (2019). *Atomic force microscopy*. Springer.

Welch, C. M., & Compton, R. G. (2006). The use of nanoparticles in electroanalysis: a review. *Analytical and Bioanalytical Chemistry*, *384*, 601–619.

Werzer, O., Kowarik, S., Gasser, F., Jiang, Z., Strzalka, J., Nicklin, C., & Resel, R. (2024). X-ray diffraction under grazing incidence conditions. *Nature Reviews Methods Primers*, *4*(1), 15.

Williams, E. (1981). *Argument Structure and Morphology. 1*(1), 81–114. https://doi.org/doi:10.1515/tlir.1981.1.1.81

Wu, H., Fu, Q., Li, Y., Cui, Y., Wang, R., Su, N., Lin, L., Dong, A., Ning, Y., & Yang, F. (2019). Controlled growth of uniform two-dimensional ZnO overlayers on Au (111) and surface hydroxylation. *Nano Research*, *12*, 2348–2354.

Xu, C., & Qu, X. (2014). Cerium oxide nanoparticle: a remarkably versatile rare earth nanomaterial for biological applications. *NPG Asia Materials*, *6*(3), e90–e90.

Xue, Y., Luan, Q., Yang, D., Yao, X., & Zhou, K. (2011). Direct evidence for hydroxyl radical scavenging activity of cerium oxide nanoparticles. *The Journal of Physical Chemistry C*, *115*(11), 4433–4438.

Yamamoto, T., Momida, H., Hamada, T., Uda, T., & Ohno, T. (2005). First-principles study of dielectric properties of cerium oxide. *Thin Solid Films*, *486*(1–2), 136–140.

Yurtcan, M. T. (2021). Deposition of grid-like single-crystal Ce2O3 thin films on LaAlO3 (100) substrate by pulsed laser deposition. *Journal of Materials Science: Materials in Electronics*, *32*(3), 3854–3862.

Zhang, G. (2013). Functional gold nanoparticles for sensing applications. *Nanotechnology Reviews*, *2*(3), 269–288.

Zhang, J. Z. (2009). *Optical properties and spectroscopy of nanomaterials*. World Scientific.

Zhou, G., Geng, W., Sun, L., Wang, X., Xiao, W., Wang, J., & Wang, L. (2019). Influence of mixed valence on the formation of oxygen vacancy in cerium oxides. *Materials*, *12*(24), 4041.

CIRRICULUM VITAE

Personal Information	
Name Surname:	Thekra Alqutamy
Date of birth:	
Birthplace:	
Nationality:	
Address:	
Tel:	
E-mail:	
Education	
High School:	Souf Camp Female Secondary School for Girls / Scientific Branch
Bachelor's degree:	Al-Bayt University of Jordan, Faculty of Science, Chemistry
Masters:	Atatürk University, Graduate School of Natural and Applied Sciences, Department of Nanoscience and Nanoengineering
Foreign Language Knowledge	
English language:	Excellent (C1)
Turkish language:	Very good (B1)
Arabic language:	Advanced (Native Language)
French language:	Elementary (A2)
Professional Organizations Membership	
Publications Produced from Thesis	
1- Alqutamy, T., Yurtcan, M. T. (2024). Growth of Cerium oxide via pulsed electron deposition as a thin film. *ICANAS 2024 Conference*, Oral Presentation. 17-20 April 2024. Antalya / Türkiye.	